BMC Genomics

RESEARCH

Open Access

Comparative study of lysine acetylation in Vesicomyidae clam *Archivesica marissinica* and the manila clam *Ruditapes philippinarum*: adaptation mechanisms in cold seep environments

Xue Kong[1,2], Wei Wang[1,2], Sunan Chen[1,2], Manzong Song[1,2], Ying Zhi[1], Yuefeng Cai[1,2], Haibin Zhang[3] and Xin Shen[1,2*]

Abstract

Background The deep-sea cold seep zone is characterized by high pressure, low temperature, darkness, and oligotrophy. Vesicomyidae clams are the dominant species within this environment, often forming symbiotic relationships with chemosynthetic microbes. Understanding the mechanisms by which Vesicomyidae clams adapt to the cold seep environment is significant. Acetylation modification of lysine is known to play a crucial role in various metabolic processes. Consequently, investigating the role of lysine acetylation in the adaptation of Vesicomyidae clams to deep-sea environments is worthwhile. So, a comparative study of lysine acetylation in cold seep clam *Archivesica marissinica* and shallow water shellfish *Ruditapes philippinarum* was conducted.

Results A total of 539 acetylated proteins were identified with 1634 acetylation sites. Conservative motif enrichment analysis revealed that the motifs -KacR-, -KacT-, and -KacF- were the most conserved. Subsequent gene ontology (GO) and Kyoto encyclopedia of genes and genomes (KEGG) enrichment analyses were conducted on significantly differentially expressed acetylated proteins. The GO enrichment analysis indicated that acetylated proteins are crucial in various biological processes, including cellular response to stimulation, and other cellular processes ($p < 0.05$ and false discovery rate (FDR) < 0.25). The results of KEGG enrichment analysis indicated that acetylated proteins are involved in various cellular processes, including tight junction, motor proteins, gap junction, phagosome, cGMP-PKG signaling pathways, endocytosis, glycolysis/gluconeogenesis, among others ($p < 0.05$ and FDR < 0.25). Notably, a high abundance of lysine acetylation was observed in the glycolysis/glycogenesis pathways, and the acetylation of glyceraldehyde 3-phosphate dehydrogenase might facilitate ATP production. Subsequent investigation into acetylation modifications associated with deep-sea adaptation revealed the specific identification of key acetylated proteins. Among these, the adaptation of cold seep clam hemoglobin and heat shock protein to high hydrostatic pressure and low temperature might involve an increase in acetylation levels. Acetylation of arginine kinase might be related to ATP production and interaction with symbiotic bacteria. Myosin heavy chain (Ama01085) has the most acetylation

*Correspondence:
Xin Shen
shenthin@163.com
Full list of author information is available at the end of the article

sites and might improve the actomyosin system stability through acetylation. Further validation is required for the acetylation modification from Vesicomyidae clams.

Conclusion A novel comparative analysis was undertaken to investigate the acetylation of lysine in Vesicomyidae clams, yielding novel insights into the regulatory role of lysine acetylation in deep-sea organisms. The findings present many potential proteins for further exploration of acetylation functions in cold seep clams and other deep-sea mollusks.

Keywords Vesicomyidae clam, Lysine acetylation, Cold seep zone, Comparative proteomics, Post-translational modification, Adaptation mechanism

Introduction

The deep sea, comprising the water column and seafloor below 200 m, constitutes two-thirds of the Earth's surface. It is distinguished from shallow water by factors such as high pressure, temperature fluctuations, heavy metals, low nutrient levels, darkness, and other environmental conditions [1, 2]. Despite the extreme environment, various organisms, including mussels [3], worms [4], crabs [5], shrimps [6], and others [7], can thrive in this habitat. These deep-sea organisms consistently establish chemosynthetic ecosystems in environments such as hydrothermal vents, cold seep zones, and habitats sustained by highly reducing sediments [8, 9].

In deep-sea ecosystems, harsh environmental characteristics prompt deep-sea species to adopt various strategies for adaptation [10]. Studies have indicated that amphipods could mitigate the adverse impacts of elevated hydrostatic pressure through the utilization of trimethylamine N-oxide, betaine, scyllo-inositol, and glycerophosphoethanolamine, enabling their survival at increased depths [11]. Sanders and Childress (1990) discovered that *Gnathophausia ingens* haemocyanin exhibits an exceptionally high affinity for oxygen and binding activity, enabling the mysid shrimp to effectively load oxygen and serve as an oxygen transporter in deep-sea environments with low levels of dissolved oxygen [12]. To enhance their efficiency in obtaining energy and nutrients from the environment, deep-sea invertebrates and chemoenergetic autotrophic bacteria have evolved a symbiotic mechanism, initially observed in the tubeworm *Riftia pachyptila* and subsequently in other species such as Vesicomyidae and Mytilidae [7, 13]. Symbiotic relationships also serve additional functions, quinone oxidoreductase was upregulated by endosymbionts, indicating that endosymbionts and mussels collaborate in sulfide detoxification [14].

Post-translational modifications (PTMs) are covalent changes to proteins that can alter their properties through cleavage or adding a modifying group to amino acids [15]. Among the major PTMs, protein acetylation was initially identified in histones [16] and is significant in activating gene transcription, signal transduction, mRNA splicing, and other cellular processes [17, 18]. Most studies on lysine acetylation have focused on mammals [19, 20], plant seeds [21, 22], and microorganisms [23, 24], whereas studies on deep-sea species are limited. Researchers presented initial findings on lysine acetylation in the hydrothermal vent shrimp *Alvinocaris longirostris*, demonstrating its involvement in various metabolic pathways, oxidative phosphorylation, and cellular processes [25]. However, a quantitative comparative analysis of acetylation modification levels is currently lacking.

Vesicomyidae clams are prominent in deep-sea chemosynthetic ecosystems, particularly in cold seep and hydrothermal vents. The clams rely on symbiotic bacteria located within their gill epidermal cells for energy and nutrients through chemosynthesis, frequently establishing symbiotic associations with chemosynthetic microbes [7]. To investigate the environmental adaptation mechanisms of Vesicomyidae clams, researchers utilized transcriptomics, genomics, and comparative proteomics techniques [26–28].

The cold seep clam *Archivesica marissinica* is an important representative species of the Vesicomyidae clams [29]. The Manila clam *Ruditapes philippinarum* belongs to the family Veneridae, which is close to the Vesicomyidae [30]. A comparative study of lysine acetylation in *Archivesica marissinica* and *Ruditapes philippinarum* was conducted to understand their adaptation to extreme environments, resulting in the identification of lysine acetylation sites in proteins. Further research on the role of lysine acetylation in Vesicomyidae clams can enhance our understanding of their adaptation to extreme deep-sea environments.

Materials and methods

Sample collection and species identification

Vesicomyidae clam *Archivesica marissinica* was obtained from South China Sea's Haima cold seep zone. The sample we used in the present study is the same as our previous article [28]. Three clams were promptly dissected and preserved at -80 ℃ upon collection on the

deck. Considering that the symbiotic microorganisms of deep sea clams exist in their gill tissues and differences between deep-sea and shallow sea environments [7], *A. marissinica* gill tissue (designated as Amgill), and muscle tissue (Ammuscle) were collected. Three individuals of the Manila clam, *Ruditapes philippinarum*, were gathered from the intertidal zone located within Haizhou Bay in Lianyungang, Jiangsu province, China, and underwent a similar processing procedure as the *A. marissinica*, except that only gill (Rpgill) tissues were collected. For LC-MS analysis, the corresponding tissues of three individuals were mixed into one pool. This was done for both species *A. marissinica* (gill and muscle tissues) and *R. philippinarum* (gill tissues).

Initially, genomic DNA was extracted from tissue using the Marine Animal Tissue Genomic DNA Extraction Kit (Code No. RR001Q, Takara, Beijing, China) for species identification. Subsequently, the cytochrome oxidase subunit I (COI) sequence was amplified utilizing the PCR Kit (Code No. RR001Q, Takara, Beijing, China). The primers employed for this amplification were COI-F (L1490: GGTCAACAAATCATAAAGATATTGG) and COI-R (H2198: TAAACTTCAGGGTGACCAAAAAAT CA) [31]. The resulting amplified fragment was ligated into a T vector using T4 DNA ligase (Code No. D2011A, Takara Bio, Beijing), followed by transformation into DH5α competent cells. Positive clones were screened utilizing Luria-Bertani (LB) medium plates supplemented with 100 μg/mL ampicillin. Subsequently, the positive clones were sent to Sangon Biotech Co., Ltd. (Shanghai) for sequencing analysis.

Protein extraction, digestion, and peptide desalination

The sample underwent protein extraction utilizing the urea lysis method (8 M Urea, 100 mM Tris/HCl, pH 8.5) as described in the literature [32]. Protein quantification was conducted utilizing the Bradford method. A total of 4 mg of proteins were obtained and dithiothreitol was subsequently added to achieve a final concentration of 10 mM. The samples were then subjected to incubation in a constant temperature mixer set at 600 rpm and 37 ℃ for a duration of 1.5 h, after which they were cooled to room temperature. Iodoacetamide was then introduced to the solution at a final concentration of 50mM and incubated in darkness for a period of 30 min. The solution was prepared by adding three times the volume of 50 mM Tris-HCl (pH 8.0) to dilute the urea concentration to 2 M. Trypsin was added to the solution at a mass ratio of 50:1 (protein: trypsin) and incubated at 37 ℃ for 15–18 h. Trifluoroacetic acid (TFA) was introduced to the solution until the final concentration reached 0.1%, and the pH was adjusted to ≤ 3 by adding 10% TFA. Desalination of peptides was performed using a C18 SPE Cartridge (Empore™ SPE Cartridges C18), followed by lyophilization of the solution.

Enrichment of acetylated peptides

After lyophilized peptides, add 1.4 mL of precooled IAP buffer (50 mM MOPS/NaOH pH 7.2, 10 mM Na_2HPO_4, 50 mM NaCl) for re-dissolution. Add pre-treated Anti-acetyl lysine antibody beads (Cat no. 13416, PTMScan Acetyl-Lysine Motif Kit, Cell Signaling Technology) to the solution. The mixture was incubated at 4 ℃ for 1.5 h, centrifuged at 2000 g for 30 s, and the supernatant was discarded. Anti-acetyl lysine antibody beads were washed three times with 1mL precooled IAP buffer and washed again three times with 1 mL pre-cooled ddH_2O. Add 40 μL 0.15% TFA to the washed Anti- Acetyl-Lysine antibody beads, incubate at room temperature for 10 min. Then add another 40 μL 0.15% TFA, and incubate for 10 min. The solution was subjected to centrifugation at 2000 g for 30 s, followed by desalination of the supernatant using C18 STAGE Tips (Cat no.13-110-055, CDS Analytical™ Empore™).

Liquid chromatography-tandem mass spectrometry (LC-MS/MS) analysis

The sample was separated using a nanoElute HPLC system (Bruker Daltonics) with a nanoliter flow rate (three technical replicates). Buffer A is 0.1% formic acid, while buffer B is 84% acetonitrile (0.1% formic acid). The sample was loaded from the automatic sampler to the loading column (Thermo Scientific Acclaim PepMap100, 100 μm*2 cm, nanoViper C18), and then separated by using analytical column (Thermo scientific EASY column, 10 cm, ID 75 μm, 3 μm, C18-A2). The analytical column was equilibrated with 95% buffer A, and linear gradient separation was performed with buffer B at a flow rate of 300 nL/min for 60 min. The samples were then subjected to the timsTOF Pro mass spectrometer (Bruker). The detection method was positive ion mode, and the ion source voltage was 1.5 kV. Both MS and MSMS were detected and analyzed using time of flight (TOF). The mass spectrometry scanning range was set to m/z 100–1700. The data collection mode was Parallel Accumulation-Serial Fragmentation (PASEF) mode. After collecting MS spectra, 10 cycles of PASEF MS/MS with a target intensity of 1.5k and a threshold of 2500 were conducted. The window time was set at 1.17 s and the charge number of MS/MS spectrum was set at 0–5. The dynamic exclusion time of MS/MS scanning was set to 24 s to avoid repeated scanning of parent ions.

Protein identification and quantification

The Peaks software [33] was utilized for database identification and quantification analysis, with database search parameters being as follows, Precursor Mass Error Tolerance: 20.00 ppm; Fragment Mass Error Tolerance: 0.05DA; Enzyme: Trypsin with [D|P]; Missed Cleavage: 2; Fixed Modifications: Carbamidomethylation; Variable Modifications: Oxidation (M); Acetyl (Protein N-term), Acetyl (K); PSM (peptide spectrum match) Filter Parameters, PSM FDR (%): 1%; Protein Filter Parameters, Proteins −10lgP: >= 20.00; Proteins Unique Peptides: >= 1; Label Free Quantification Parameters, Mass Error Tolerance: 20.00 ppm; Retention Time Shift Tolerance: 1.00 min. The *A. marissinica* genome data (specifically its annotated protein data) we referred to comes from previous articles [27].

Further analyses of modified peptides and proteins containing modified peptides

Cluster analysis of modified peptide

Firstly, the quantitative data of the target peptide was standardized to the (-1,1) range. Subsequently, the Complexheatmap R package (R Version 3.4, https://bioconductor.org/packages/release/bioc/html/ComplexHeatmap.html) was employed to categorize the samples and the peptide expression levels concurrently (Euclidean distance algorithm and Average linkage connection method), resulting in the creation of hierarchical clustering heatmaps.

Conservative motif analysis

Sequence information encompassing 6 amino acids both upstream and downstream of modification sites, totaling 13 amino acids in length, was acquired. This information was subsequently employed to forecast potential conservative motifs utilizing the MeMe website (http://meme-suite.org/index.htm.), with parameter settings including a width of 13, occurrence of 50, and background species.

Subcellular localization analysis of proteins containing modified peptide

The CELLO tool [34] was utilized for predicting subcellular localization, employing a machine learning technique known as multi-class Support Vector Machine to analyze protein sequence data with established subcellular localization information from a public database. This approach was employed to forecast the subcellular localization of the target protein.

Protein domain analysis of proteins containing modified peptide

The Pfam database [35] was utilized for the analysis of protein domains, which are represented as a collection of protein families in the form of multiple sequence alignments and Hidden Markov Models. This database also includes domain information. The InterProScan software package (https://www.ebi.ac.uk/interpro) was employed to apply scanning algorithms on the InterPro database in order to search for functional characterization of sequences, ultimately obtaining domain annotation information for target protein sequences within the Pfam database.

Gene ontology function annotation

Blast2GO was utilized for the Gene Ontology (GO) annotation (http://www.geneontology.org/) of target protein sets, encompassing four primary procedures: sequence alignment (Blast), extraction of GO terms (Mapping), annotation of GO terms (Annotation), and additional InterProScan annotation (Annotation Augmentation).

Kyoto encyclopedia of genes and genomes pathway annotation

The KAAS (KEGG Automatic Annotation Server, http://www.genome.jp/kegg/) software was utilized to conduct KEGG pathway annotation on the specified protein sets.

Enrichment analysis

The Fisher's Exact Test was employed to assess the distribution of various Gene Ontology (GO) terms within the target protein set compared to the overall protein set, followed by GO annotation enrichment analysis on the target protein set. Multiple comparisons were corrected using the False Discovery Rate (FDR). Protein domain terms, GO terms, and KEGG terms meeting the criteria of a p-value < 0.05 and false discovery rate (FDR) < 0.25 were considered to be statistically significant.

Analysis of protein-protein interaction network

The researchers utilized the STRING database (http://string-db.org/) to identify direct and indirect interaction relationships among target proteins. The resulting interaction network was then constructed and analyzed using Cytoscape software (version 3.2.1) [36].

Structure and evolution analyses of key acetylated proteins

The tertiary structure and evolutionary relationships of key acetylated proteins (arginine kinase, hemoglobin, heat shock protein, carbonic anhydrase and myosin heavy chain) were examined through the analysis of their amino acid sequences obtained from a database. Protein sequence alignment was performed using Clustal W software (version 1.83) [37]. Phylogenetic trees were obtained by using MEGA v4.0 software, and amino acid sequences were used to construct a molecular phylogenetic tree

based on neighbor-joining method, with bootstrap values set to 1000 replicates [38]. The tertiary structure of acetylated proteins was predicted using the SWISS-MODEL program (http://swissmodel.expasy.org/) and then visualized by using Deepview/Swiss-Pdb Viewer version 4.0 (https://spdbv.vital-it.ch/).

Results

Species identification

After obtaining the COI sequences of deep-sea and shallow-sea organisms, this information was archived in the supplementary files of previous articles (https://www.frontiersin.org/journals/marine-science/articles/https://doi.org/10.3389/fmars.2023.1294736/full#supplementary-Material) [28]. We conducted an online BLAST analysis (https://blast.ncbi.nlm.nih.gov/Blast.cgi). The results (not shown) indicated that deep-sea shellfish exhibited the highest degree of similarity with *A. marissinica*, showing a 100% match. In a similar manner, the species of shallow-water shellfish has been conclusively identified as *R. philippinarum*, exhibiting a 100% similarity.

Overview of the acetylome data

The experimental procedures were outlined in Fig. 1a. As illustrated in Fig. 1b, the peptide mass error for the identified acetylated peptides predominantly fell within a 10 ppm range, suggesting the accuracy and reliability of the identification outcomes. The Andromeda score of mass spectrometry MS2 of acetylated peptides was notably favorable, with over 62.21% of modified peptides achieving scores exceeding 60 points, and the median score for peptides being 67.69 points (Fig. 1d). Most acetylated peptides exhibited lengths ranging from 7 amino acids (aa) to 19aa, with the 11aa-13aa range being the most prevalent (Fig. 1c).

To analyze the acetylation modification identification of inter groups, Venn diagrams were used to analyze the overlap between the groups. Specifically, 419 acetylated proteins were found to be present in Ammuscle, Amgill, and Rpgill (Fig. 2a). Additionally, about 963 acetylated peptides co-existed in the above three groups (Fig. 2b). Then, we analyzed repeatability within each group, finding that the number of acetylated peptides identified in the three technical replicates within each group exceeded 992, representing over 90% (Fig. S1a1-c1). Furthermore, the number of acetylated proteins exceeded 400 in all cases, accounting for more than 93% (Fig. S1a2-c2).

Motif characteristics of acetylated peptides in *A. marissinica* and *R. philippinarum*

A statistical examination was conducted on the acetylation sites of all identified proteins. Figure 3a showed that about 300 proteins exhibited one sites (in total 540 proteins), with the Ama01085 protein displaying 149 modification sites (containing duplicate sites). Subsequently, conservative motifs were investigated by analyzing the frequency distribution of the six amino acids preceding and following the acetylation modification site on the modified peptides. The results demonstrated that the most prevalent conserved motifs were -EK-, -KR-, and -KK-, as illustrated in Fig. 3b. Subsequently, enrichment and statistical analysis were performed on the conserved motifs, revealing that -KacR-, -KacT-, and -KacF- exhibited the highest frequency of occurrence, all positioned at +1 (refer to R, T, and F, Fig. 3c). Figure 3d showed that the top 3 motif (enrichment statistics) were the same as that of Fig. 3c.

Quantitative analysis of acetylated peptides from *A. marissinica* and *R. philippinarum*

A Fold Change ≥ 2.0 or ≤ 0.5 and a P value < 0.05 (T-test) were established as criteria, facilitating the determination of upregulated and downregulated modified peptides between groups. Figure 4 illustrates that the comparative group Rpgill vs. Amgill exhibited 581 differentially expressed acetylated peptides,

and Ammuscle vs. Amgill had 702 differentially expressed peptides (Table S1-1, Table S1-2). Figure 4b and c show that the significantly differentially expressed acetylated peptides obtained through the above screening criteria could effectively separate the comparative groups.

Functional annotation and enrichment of differentially expressed acetylated proteins

Analysis of Rpgill vs. Amgill

Most of these differentially expressed proteins (actually differentially expressed peptides) from Rpgill vs. Amgill comparison group were found to be located in the cytoplasmic (37%) and nuclear (36%) compartments (Fig. 5a). Subsequently, Fisher's Exact Test was utilized to perform domain enrichment analysis. The sole domain found to be significantly enriched was the myosin tail ($p = 0.038$), although its false discovery rate (FDR) exceeded 0.25 (Fig. 5b).

GO were conducted on proteins harboring differentially expressed modified peptides in the Rpgill vs. Amgill comparison group. No statistically significant enrichment of biological processes was observed in Fig. 6a 1. Similar situations also exist in molecular function and cellular component (Fig. 6b1, c1). Then, the focus was on the upregulated proteins from comparative group Rpgill vs. Amgill. Notably, the biological process exhibited significant enrichment ($p < 0.05$ and FDR < 0.25), with the top five processes identified as microtubule-based

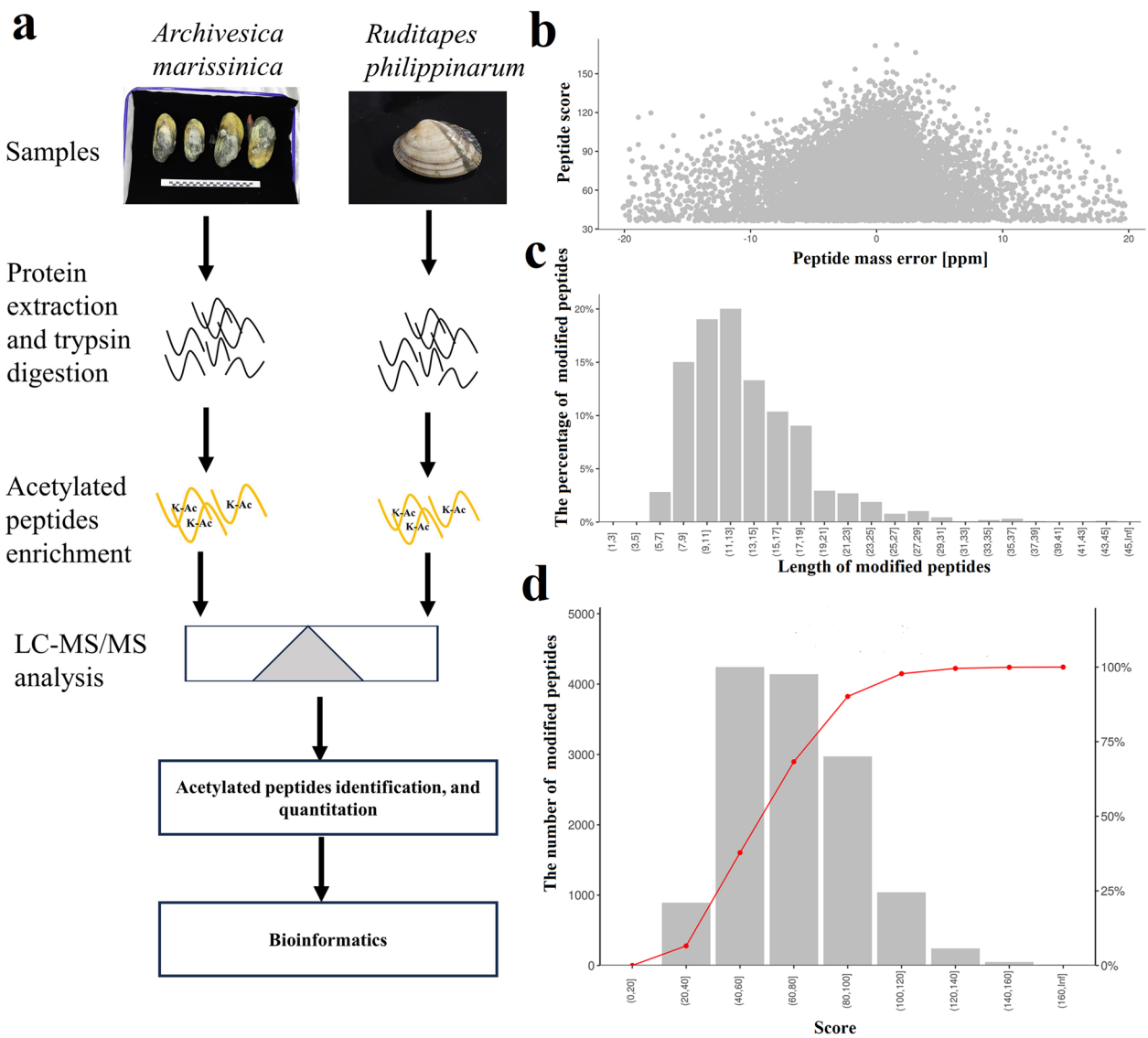

Fig. 1 Overview of the global identification of lysine acetylation sites in *Archivesica marissinica* **a** General workflow for acetylome analysis. **b** Mass error of the modified peptides. **c** Length distribution of the modified peptides. **d** The MS2 Andromeda score of the modified peptides

process, signaling, signal transmission, cell communication, and cellular response to stimulation (Fig. 6a2). The five most enriched molecular functions, as determined by statistical significance ($p < 0.05$ and FDR < 0.25), were guanyl riboside binding, GTP binding, nucleoside binding, riboside binding, and guanyl nucleoside binding (Fig. 6b2). The cellular components were significantly enriched ($p < 0.05$ and FDR < 0.25), and the top five were intracellular non-membrane-bounded organelle, non-membrane-bounded organelle, organelle, intracellular organelle, and cytoskeleton (Fig. 6c2). For downregulated proteins. In enrichment analysis, only $p < 0.05$ was found for terms generation of precursor metabolites and energy (biological process), but its FDR > 0.25 (Fig. 6a3). Enrichment analysis of molecular function revealed statistical significance ($p < 0.05$) for enzyme activity, transition metal ion binding, zinc ion binding, hydro enzyme activity, and carbon oxygen enzyme activity, with an FDR exceeding 0.25 (Fig. 6b3). The cellular components by quantity were showed in Fig. 6a3, none of which exhibited significant enrichment (Fig. 6c3).

This study performed a KEGG pathway annotation and enrichment analysis on proteins harboring differentially expressed acetylated peptides from the comparative groups of Rpgill vs. Amgill. KEGG pathway enrichment analysis showed significant changes ($p < 0.05$)

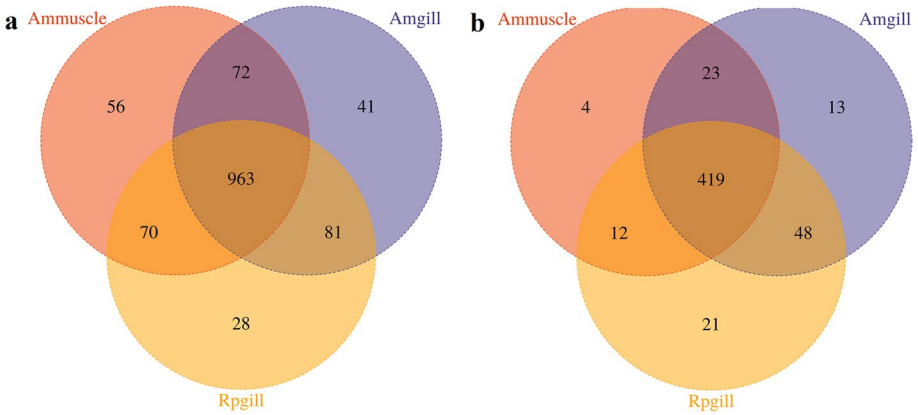

Fig. 2 The Venn diagram of the peptides and proteins containing acetylation sites in *Archivesica marissinica* and *Ruditapes philippinarum* (between groups). **a** The Venn diagram of the peptides containing acetylation sites. **b** The Venn diagram of the proteins containing acetylation sites

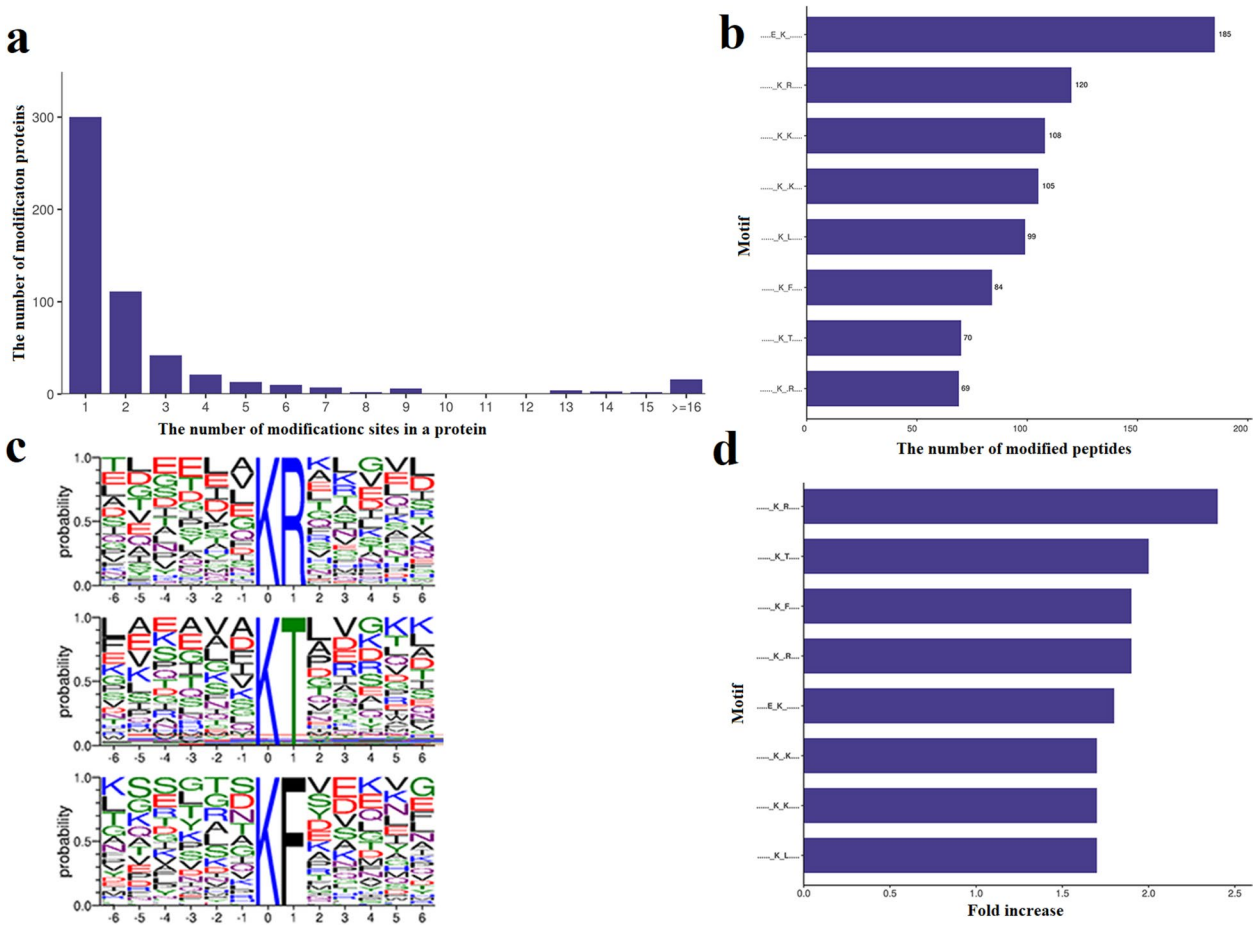

Fig. 3 Characteristics of the lysine acetylation motifs in *Archivesica marissinica*. **a** Distribution of the number of the lysine acetylation sites in a protein. **b** The number of modified peptides containing specific motif (top 8). **c** Enriched acetylation motif logos. The size of each letter represents the frequency of the amino acid residue in that position. **d** Conservative motif enrichment statistics (top 8). The X-axis represents the ratio of the number of identified acetylated peptides (contain specific motif) corresponding to the number of theoretical peptides (contain specific motif)

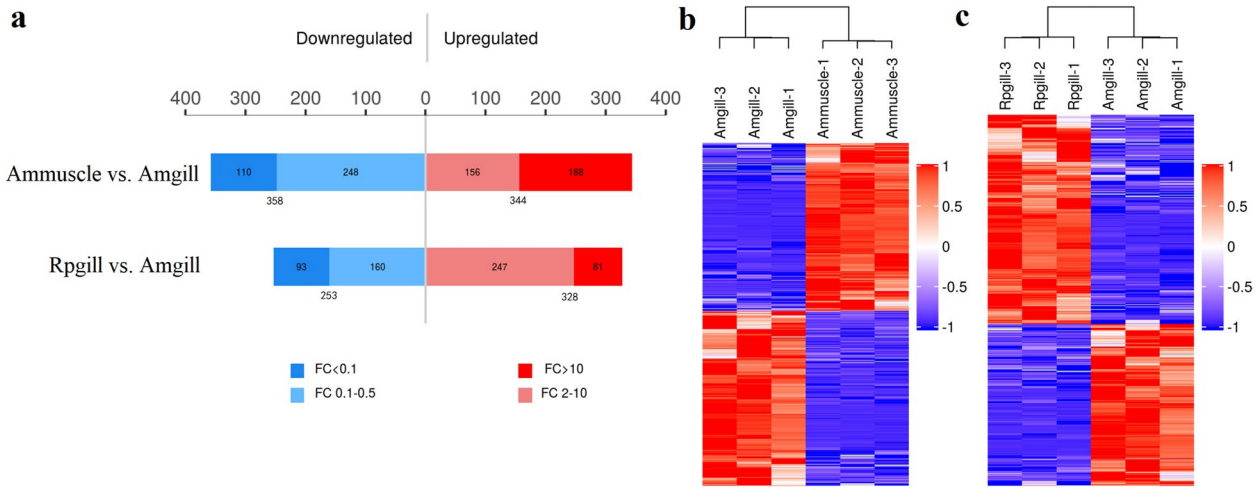

Fig. 4 Histogram of the quantitative differential acetylated peptides and hierarchical cluster analysis of the differentially expressed acetylated peptides. **a** Histogram of the quantitative differential acetylated peptides. **b** Hierarchical cluster analysis of the differentially expressed acetylated peptides (Ammuscle vs. Amgill). **c** Hierarchical cluster analysis of the differentially expressed acetylated peptides (Rpgill vs. Amgill). FC means fold change. Each column represents a sample, and each row represents an acetylated peptide

Table 1 The identification and quantitation of acetylated sites, peptides, and proteins in *Archivesica Marissinica* and *Ruditapes Philippinarum*

Acetylated Sites		Acetylated Peptides		Acetylated Proteins	
Identified	Quantified	Identified	Quantified	Identified	Quantified
1639	1634	1311	1308	540	539

in important pathways such as tight junction, motor proteins, apoptosis, and tryptophan metabolism, but FDR of these pathways exceeded 0.25 (Fig. 7a1). Subsequently, KEGG pathway annotation and enrichment analysis were conducted on the upregulated proteins. Notably, tight junction, motor proteins, gap junction, phagosome, cGMP-PKG signaling pathway, Ras signaling pathway, and endocytosis pathways were found to be significantly

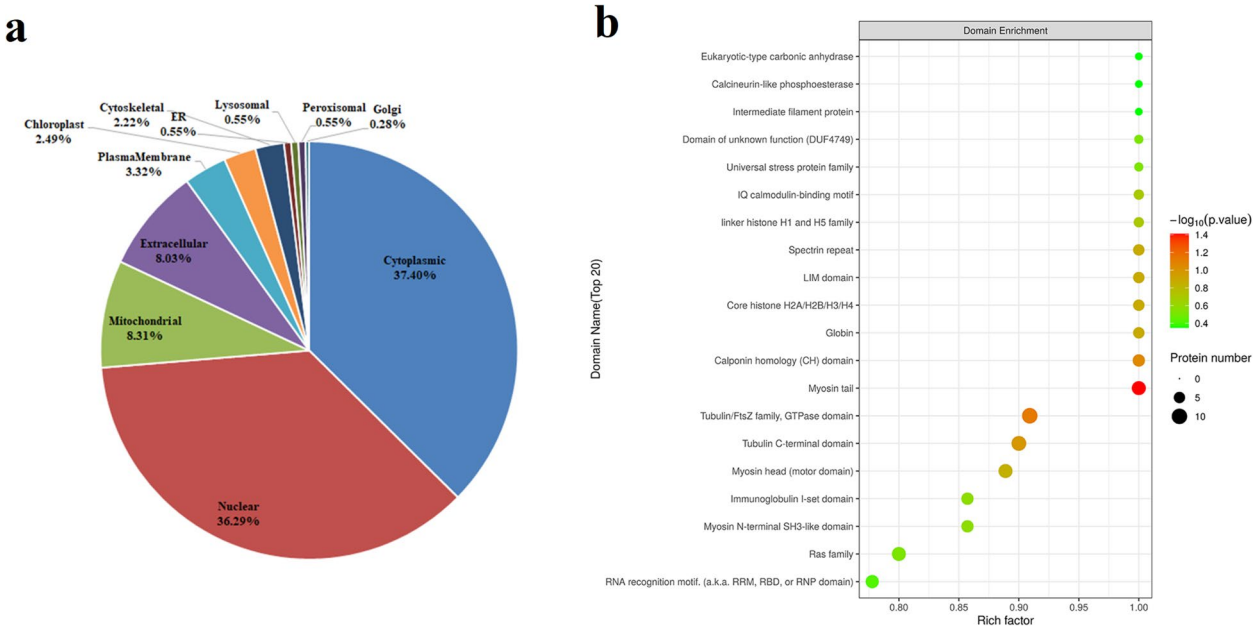

Fig. 5 Subcellular localization and domain analysis of the differentially expressed acetylated proteins for *Ruditapes philippinarum*'gill (Rpgill) vs. *Archivesica marissinica*'gill (Amgill). **a** Subcellular localization of the differential expressed acetylated proteins. **b** Domain enrichment analysis of the differential expressed acetylated proteins

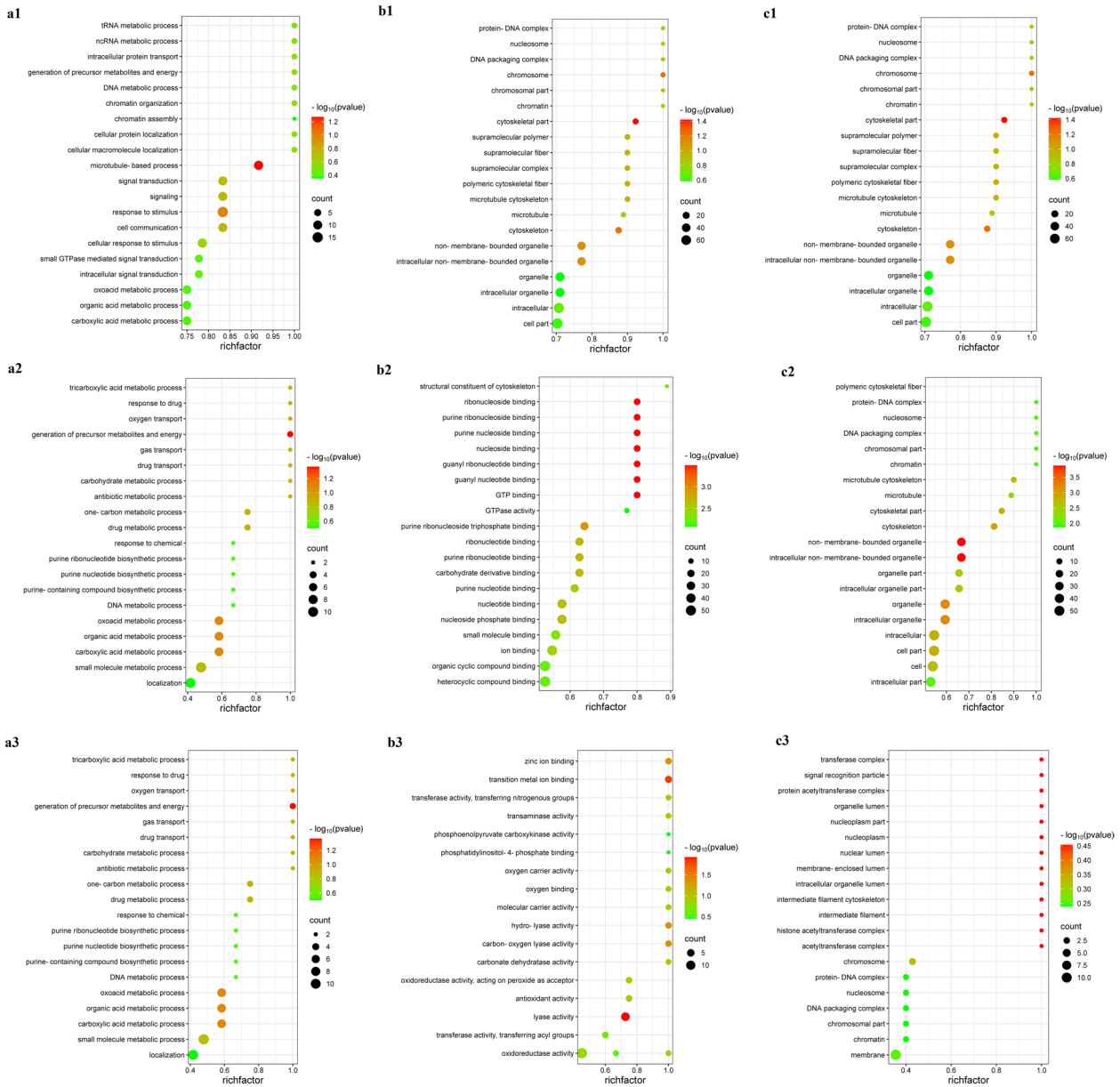

Fig. 6 GO analysis related maps of differentially expressed acetylated proteins from *Ruditapes philippinarum*'gill (Rpgill) vs. *Archivesica marissinica*'gill (Amgill). **a1**, **a2**, **a3** Biological process enrichment bubble map of all differential proteins, upregulated proteins and downregulated proteins, respectively. **b1**, **b2**, **b3** Molecular function enrichment bubble map of all differential proteins, upregulated proteins and downregulated proteins, respectively. **c1**, **c2**, **c3** Cellular component enrichment bubble map of all differential proteins, upregulated proteins and downregulated proteins, respectively

enriched ($p < 0.05$ and FDR < 0.25) (Fig. 7a2). Then, KEGG pathway analysis was performed on the downregulated proteins. Pathway enrichment analysis revealed notable alterations in key pathways such as tryptophan metabolism, biosynthesis of cofactors, and glycolysis/gluconeogenesis ($p < 0.05$ and FDR < 0.25) (Fig. 7a3, Fig. 8). The acetylated proteins implicated in differentially significant KEGG pathways are documented in Table S2.

Analysis of Ammuscle vs. Amgill

Most of these differentially expressed peptides from the comparative group Ammuscle vs. Amgill. were found to be located in the cytoplasmic (42%) and nuclear (27%) (Fig. S2a). Subsequently, the domains of proteins containing differentially expressed acetylated peptides were predicted. Then Fisher's exact test was utilized for domain enrichment analysis. The only domain that was

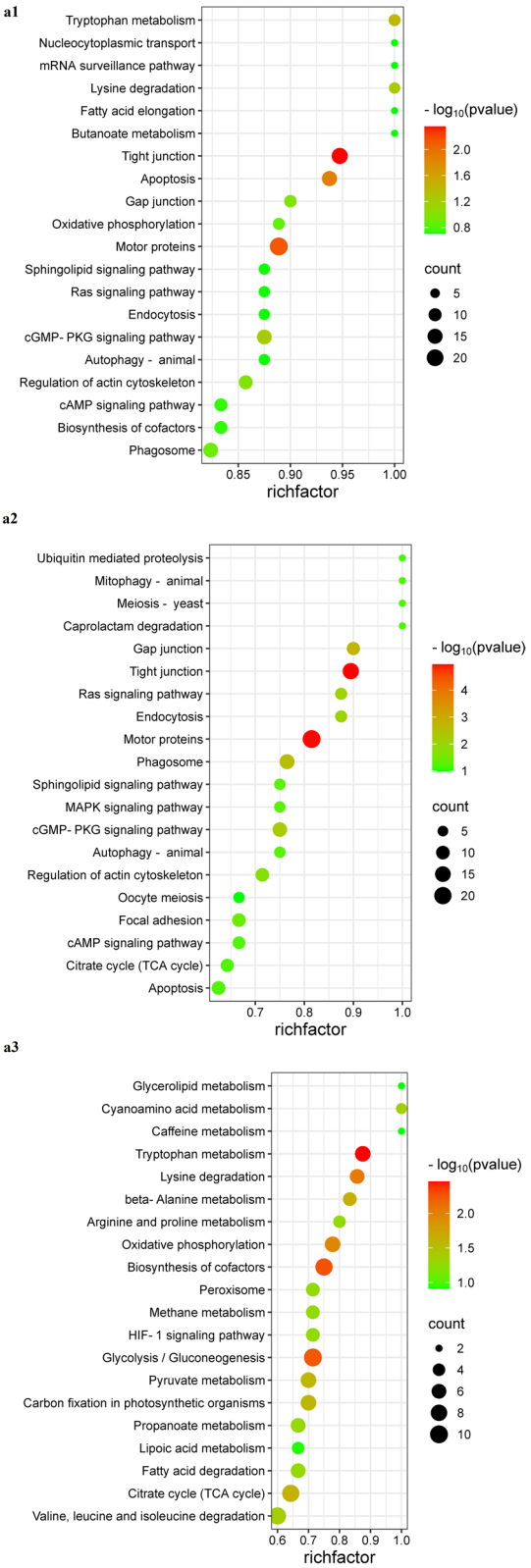

◀ **Fig. 7** Kyoto Encyclopedia of Genes and Genomes pathway analysis of differentially expressed acetylated proteins for Rpgill vs. Amgill. **a1**, **a2**, **a3** KEGG pathway enrichment bubble map of all differential proteins, upregulated proteins and downregulated proteins, respectively

significantly enriched was myosin tail ($p = 0.029$), but its FDR exceeded 0.5 (Fig. S2b).

GO functional annotation and enrichment analysis were performed on proteins containing differentially expressed acetylated peptides in the comparative group Ammuscle and Amgill. No biological processes were found to be significantly enriched, with p-values greater than 0.05 and FDR values exceeding 0.25 (Fig. S3a1). Enrichment analysis of molecular functions revealed that the p-values for adenyl nucleotide binding and adenyl ribonucleotide binding were both less than 0.05, while the FDR was greater than 0.25 (Fig. S3b1). In terms of cellular components, none of these cellular components showed significant enrichment ($p > 0.05$ and FDR > 0.25) (Fig. S3c1).

Subsequently, it was for downregulated proteins from Ammuscle vs. Amgill. In enrichment analysis of biological processes, only the cellular nitrogen compound metabolic process demonstrated $p < 0.05$, but the FDR > 0.25 (Fig. S3a2). The p-value of structural constituent of ribosome, protein dimerization activity, DNA binding, protein heterodimerization activity, and nucleic acid binding (molecular functions) were less than 0.05, but their FDR > 0.25 (Fig. S3b2). Additionally, cellular component enrichment analysis indicated that the p-values for the ribonucleoprotein complex, ribosome, nucleosome, chromatin, and DNA packaging complex were all less than 0.05, with the FDR exceeding 0.25 (Fig. S3c2).

Next, the downregulated protein was examined. Enrichment analysis of biological processes revealed that only the cellular nitrogen compound metabolic process showed a significance level of $p < 0.05$, but the FDR was > 0.25 (Fig. S3a3). In the enrichment analysis of molecular functions, the p-values for structural constituent of ribosome, protein dimerization activity, protein heterodimerization activity, DNA binding, and nucleic acid binding were all less than 0.05, while FDR exceeded 0.25 (Fig. S3b3). The analysis of cellular components showed that the p-values for the ribonucleoprotein complex, ribosome, nucleosome, chromatin, and DNA packaging complex were all below 0.05, while FDR values were greater than 0.25 (Fig. S3c3).

The KEGG pathway annotation and enrichment of proteins containing differentially acetylated modified peptides from Ammuscle vs. Amgill were analyzed. Significant changes were observed in key pathways such as

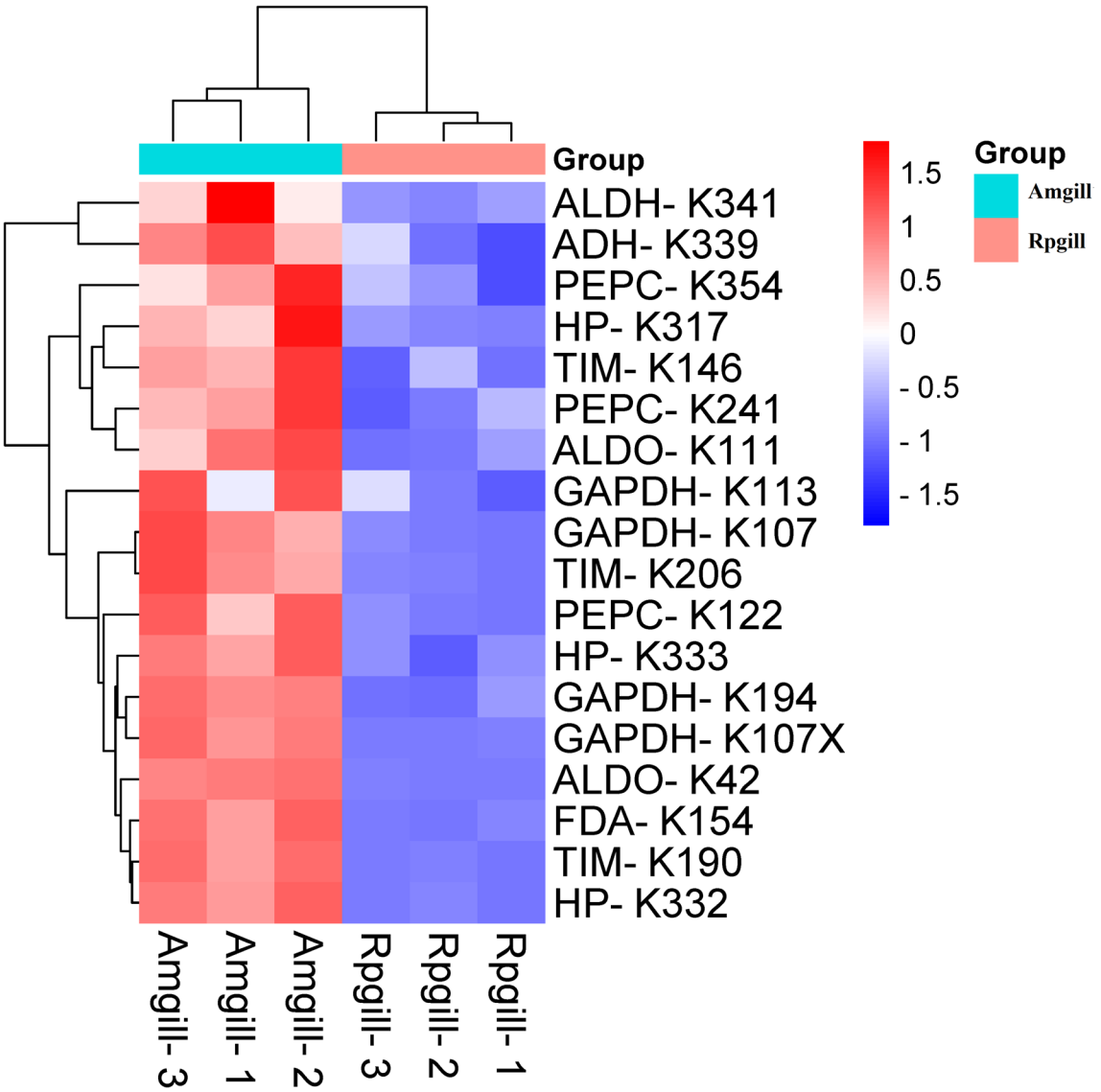

Fig. 8 Multiple enzymes involved in the KEGG pathway Glycolysis/Gluconeogenesis (Amgill/Rpgill). Notes: ADH, alcohol dehydrogenase; ALDH, aldehyde dehydrogenase; ALDO, aldolase; FDA, fructose-1, 6-bisphosphate aldolase; GAPDH, glyceraldehyde 3-phosphate dehydrogenase; HP, hypothetical protein LOTGIDRAFT_201812; PEPC, Phosphoenolpyruvate carboxykinase; TIM, triosephosphate isomerase

pyruvate metabolism, glycolysis and gluconeogenesis, tryptophan metabolism, lysine degradation, and methane metabolism ($p < 0.05$), but the FDR of the above pathways exceeded 0.25 (Fig. S4a1). Subsequently, KEGG pathway analysis was performed on the upregulated proteins. Further analysis demonstrated significant enrichment ($p < 0.05$ and FDR < 0.25) in glycolysis/gluconeogenesis, motor proteins, focal adhesion, carbon fixation in photosynthetic organisms, cGMP-PKG signaling pathway, and regulation of actin cytoskeleton (Fig. S4a2). Then, the analysis was on downregulated proteins. Pathway enrichment analysis revealed significant alterations in tryptophan metabolism, ribosome, and lysine degradation ($p < 0.05$ and FDR < 0.25) (Fig. S4a3). Acetylated proteins involved in differentially significantly KEGG pathways were listed in Table S3.

Interaction network of differentially expressed acetylated proteins in *A. marissinica* and *R. philippinarum*

Protein-protein interaction network analysis was performed on proteins containing differentially acetylated peptides from the comparative groups Rpgill and Amgill. A total of 339 proteins were involved in this network

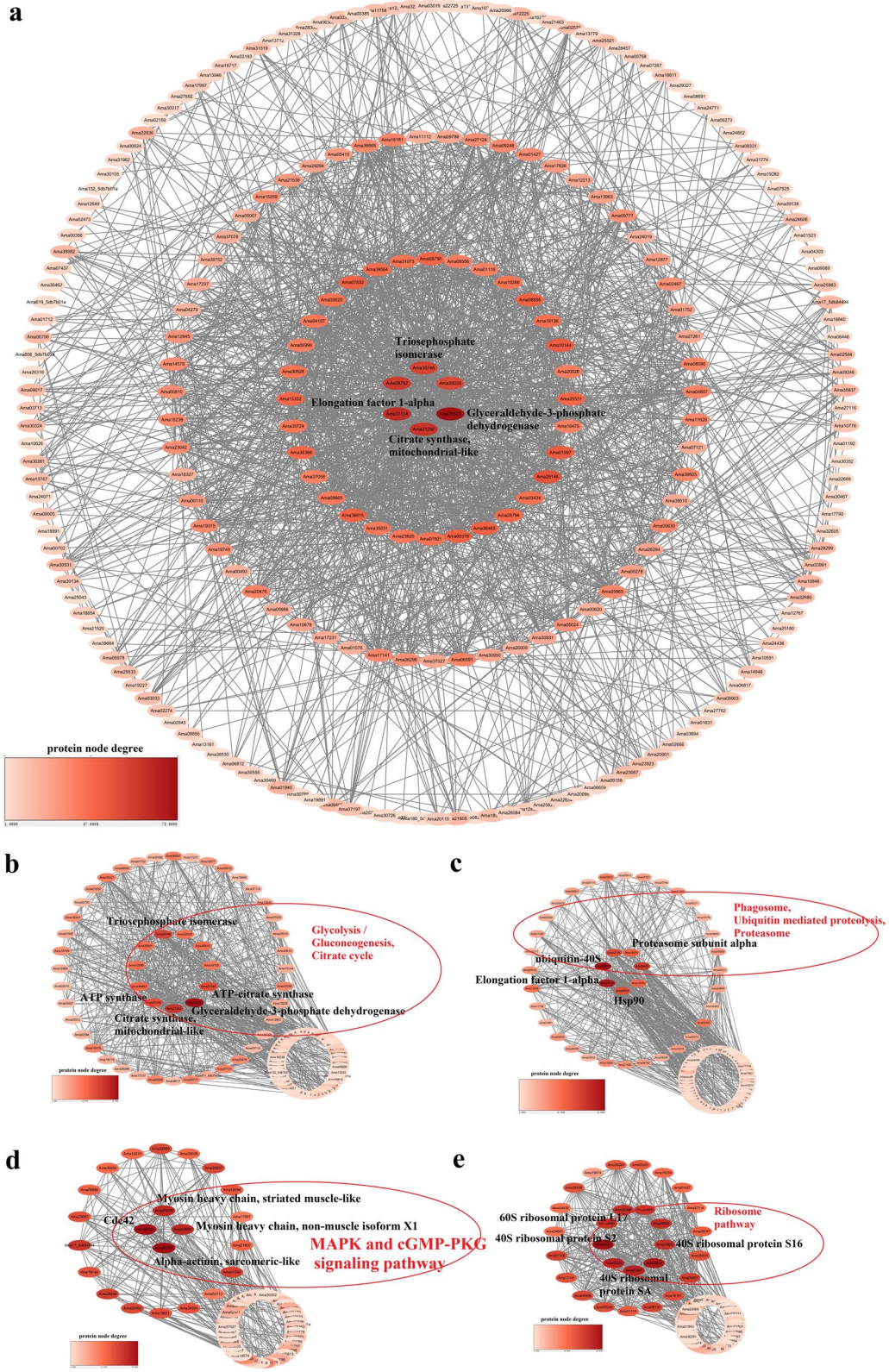

Fig. 9 Protein interaction network of differentially expressed acetylated proteins from Rpgill vs. Amgill. **a** Protein interaction network of all differentially expressed acetylated proteins. **b**, **c**, **d**, **e** Protein interaction network of four distinct clusters

(Fig. 9a, Table S4-1). Subsequently, utilizing the principle of topology recognition, proteins exhibiting high connectivity within the interaction network were categorized into four distinct clusters (Fig. 9b, c, d and e, Table S4-2, S4-3, S4-4, S4-5). Cluster 1 (Fig. 9b, Table S4-2) was primarily associated with glucose metabolism, including glycolysis/gluconeogenesis, citrate cycle (TCA cycle), and others. Cluster 2 was primarily pertained to protein degradation processes, encompassing pathways such as phagosome, ubiquitin mediated proteolysis, and proteasome (Fig. 9c, Table S4-3). Cluster 3 was predominantly associated with signal transduction mechanisms, including pathways such as MAPK and cGMP-PKG signaling pathway (Fig. 9d, Table S4-4). Cluster 4 was primarily linked to the Ribosome pathway (Fig. 9e, Table S4-5).

The protein-protein interaction network was also analyzed on the proteins containing the differentially acetylated peptides of the comparative group Ammuscle vs. Amgill. A total of 327 proteins were involved in this network (Fig. S5a, Table S5-1). The interaction network was divided into five clusters (Fig. S5b, S5c, S5d, S5e, S5f, Tables S5-2, S5-3, S5-4, S5-5, S5-6). Cluster 1 (Fig. S5b, Table S5-2) was primarily associated with signal transduction pathways, such as the MAPK and cGMP-PKG signaling pathway. Cluster 2 was primarily associated with ribosome metabolism (Fig. S5c, Table S5-3), while Cluster 3 was mainly linked to glucose metabolism, fatty acid metabolism, and amino acid metabolism, encompassing glycolysis/gluconeogenesis, citric acid cycle (TCA cycle), Fatty acid biosynthesis, arginine biosynthesis, glycine-serine-threonine metabolism, as well as valine-leucine-isoleucine degradation (Fig. S5d, Table S5-4). Cluster 4 and Cluster 5 exhibited a limited number of members.

Acetylation associated with cold seep adaptation in *A. marissinica*

The experimental findings indicate focuses on specific acetylated proteins, including arginine kinase (AK), carbonic anhydrase (CA), hemoglobin, heat shock protein, and myosin heavy chain. Two arginine kinases were identified in the comparative groups: AmAK1 (Ama35642) and AmAK2 (Ama07197). AmAK1 was classified as a two-domain arginine kinase, while AmAK2 comprised a single domain, as illustrated in the evolutionary tree (Fig. 10b). Sequence alignment analysis revealed that both AmAK1 and AmAK2 exhibit conserved motifs characteristic of arginine kinases. In the comparison between Rpgill and Amgill, AmAK1 exhibited six acetylation sites, with K316, K454, and K534 significantly downregulated and K388 significantly upregulated. K316 and K454 are in random coil, while K388 and K534 are in beta-sheet. AmAK2 contained four acetylation sites, with K324 significantly downregulated and K294 and K351 significantly upregulated. All three sites are located in alpha-helix (Table S6-1 and Fig. 10c). In the comparative groups Ammuscle vs. Amgill, AmAK1 was identified as having six acetylation sites, with only two sites (K454 and K534) significantly downregulated in expression. AmAK2 was identified to have four acetylation sites, with only one site (K294) significantly upregulated in expression (Table S6-2). All three sites are in alpha-helix. In the comparison between Ammuscle and Amgill, AmAK1 displayed six acetylation sites, with only two sties significantly downregulated (K454 and K534). AmAK2 demonstrated four acetylation sites, with only one site significantly upregulated (K294) (Table S6-2).

Two CAs (Amca1 and Amca2) were found in the comparative groups. They belong to one-domain carbonic anhydrases, as shown in the evolutionary tree (Fig. S6b). Sequence alignment revealed conserved motifs of CA in Amca1 and Amca2 (Fig. S6a). In the comparison group Rpgill vs. Amgill, Amca1 was identified with nine acetylation sites, with seven sites showing significant differential expression (K66, K66, K81, K86, K100, K100, K185). Seven sites were significantly downregulated, with K66 and K86 in random coil and K81, K100, and K185 in beta-sheet. Amac2 showed ten acetylation sites, with six downregulated sites (S2, K50, K65, K65, K69 and K84) and no upregulated sites. In addition, S2, K50, and K69 are in random coil, while K65 and K84 are in beta-sheet (Table S6-1 and Fig. S6c, S6d). In the comparison between Ammuscle and Amgill, Amac1 exhibited nine acetylation sites, with eight significantly downregulated (K66, K66, K66, K81, K86, K100, K100 and K185) and none significantly upregulated. Amac2 contained eight acetylation sites, with seven significantly downregulated (K50, K50, K50, K65, K65, K69 and K84) (Table S6-2).

Two hemoglobins (AmHbI and AmHbII) were identified from the comparison groups. AmHbI displayed 18 acetylation sites, with 16 sites showing significant differential expression in the comparison group Rpgill vs. Amgill. One site (K46) was upregulated, while 15 sites (V2, K8, K8, K16, K28, K32, K32, K35, K46, K46, K56, K56, K56, K56 and K91) were downregulated. All sites, except for V2 in the random coil, are in alpha-helix. AmHbII has one acetylation site (K36) that is downregulated and in alpha-helix (Table S6-1, Fig. S7c, S7d). In the comparison between Ammuscle and Amgill, AmHbI exhibited 18 acetylation sites, with 15 significantly downregulated sites located in the alpha-helix (V2, K8, K8, K16, K28, K32, K35, K46, K46, K46, K46, K56, K91 and K91), while AmHbII demonstrated one downregulated acetylation site at K36 in the alpha-helix (Table S6-2, Fig. S7c, S7d).

Four heat shock proteins were found in the comparison groups: Amhsp22, Amhsp70-1, Amhsp70-2, and

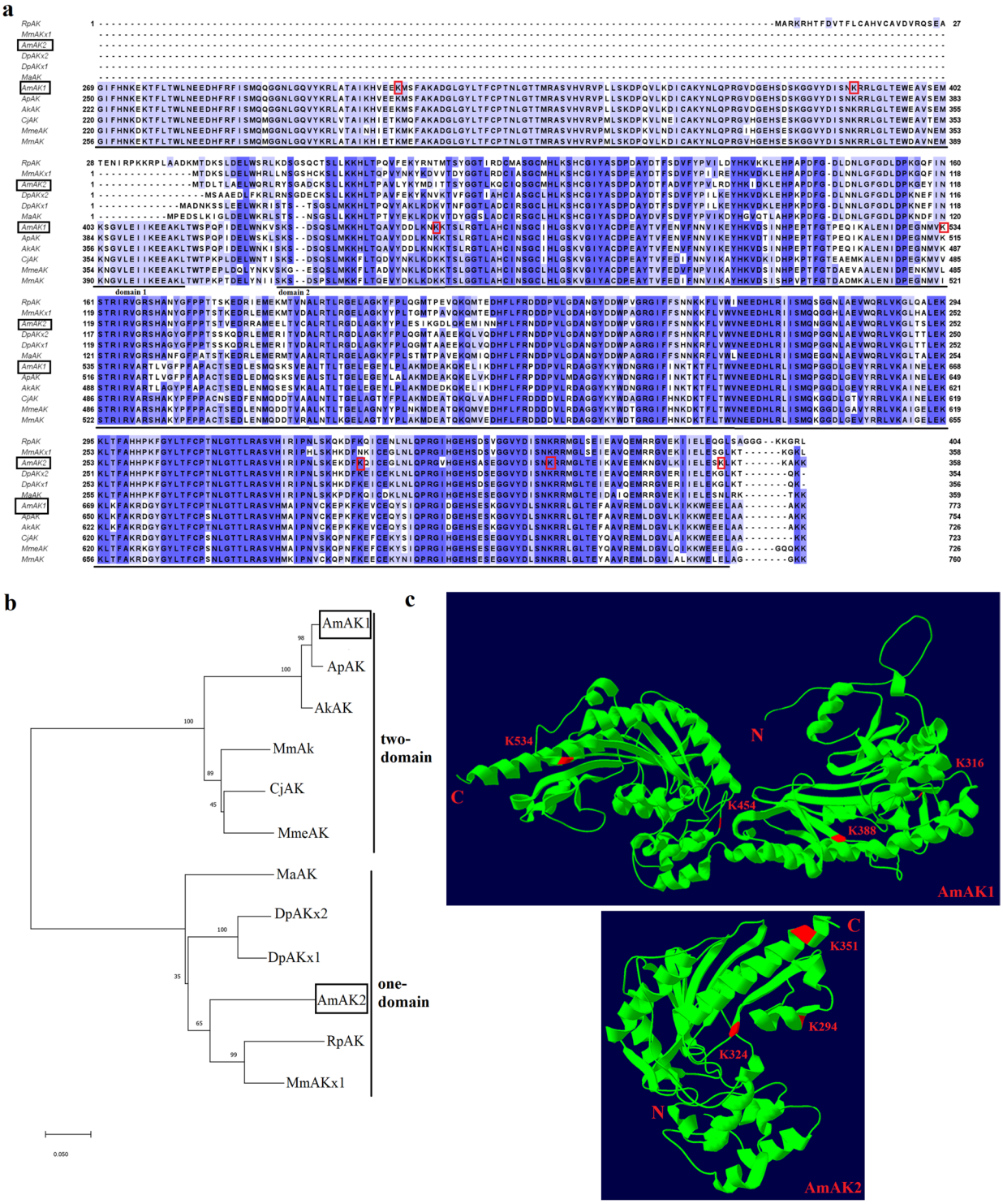

Fig. 10 Sequence alignment by clustalW, evolutionary tree based on neighbor-joining method, and tertiary structure of arginine kinases (AK) from selected mollusks species. **a** Sequence alignment of arginine kinases from *Archivesica marissinica* (AmAK1, Ama35642; AmAK2, Ama07197), *Archivesica packardana* (ApAK, AXE71657.1), *Abyssogena kaikoi* (AkAK, BAE16974.1), *Mercenaria mercenaria* (MmAK, XP_045197745.1), *Corbicula japonica* (CjAK, BAB91357.1), *Meretrix meretrix* (MmeAK, ACP43444.1), *Ruditapes philippinarum* (RpAK, XP_060608460.1), *Mercenaria mercenaria* (MmAKx1, XP_045196942.1), *Dreissena polymorpha* (DpAKx2, XP_052244383.1; DpAKx1, XP_052244382.1), and *Mya arenaria* (MaAK, XP_052811049.1). Deep blue represents 100% similarity, light purple represents 30% similarity, the color between the two represents 100%-30%. **b** Phylogenetic tree of arginine kinases. **c** Predicted tertiary structure of arginine kinases. The acetylation sites and N, C terminal of proteins are marked in red

Amhsp90. In the comparison group Rpgill vs. Amgill, Amhsp22 was found to have six acetylation sites, with K93 significantly upregulated and K100 and K111 significantly downregulated. K93 is in a random coil, while K100 and K111 are in a beta-sheet. Amhsp70-1 showed one acetylation site at K364, which is located in an alpha-helix and showed increased expression. Amhsp70-2 displayed six acetylation sites, with K71 and K246 showing significant differential expression. K71 was upregulated and K246 was downregulated, both located in the alpha-helix. Amhsp90 has eight acetylation sites, with K214 showing significant upregulation on the beta-sheet (Table S6-1, Fig. S8b, S8c, S8d, S8e). In the comparison between Ammuscle and Amgill, Amhsp22 displayed six acetylation sites, with 4 showing significant upregulation (K93, K100, K100 and K134). K93 and K134 are in random coil, while K100 is in beta-sheet. Amhsp70-1 demonstrated one acetylation site (K364) that was significantly downregulated and located in the alpha-helix. Amhsp70-2 has six acetylation sites, with three sites (K246, K246 and K348) significantly downregulated. K246 and K348 are in alpha-helix. Amhsp90 has four acetylation sites, with two sites (K196 and K441) significantly downregulated in alpha-helix (Table S6-2, Fig. S8b, S8c, S8d, S8e).

The results showed that Ama01085 has the most acetylation sites and is identified as a myosin heavy chain. After filtering, four myosin heavy chains were found: AmMyHC1 (Ama01085), AmMyHC2 (Ama02678), AmMyHC3 (Ama01076), and AmMyHC4 (Ama00622). AmMyHC1-3 are muscle types, while AmMyHC4 is a non-muscle type (Fig. S9a). In the Rpgill vs. Amgill group, AmMyHC1 exhibited 72 acetylation sites, with 30 sites showing significant differences-14 downregulated and 16 upregulated (Table S6-1 and Fig. S9b). In the Ammuscle vs. Amgill group, AmMyHC1 displayed 77 acetylation sites, with 57 sites showing significant differences-2 downregulated and 55 upregulated (Table S6-2, Fig. S9b). Moreover, numerous modification sites exist for AmMyHC2, 3, and 4, as listed in Table S6 and shown in Fig. S9b-S9e.

Discussion

In this study, researchers compared acetylation in *A. marissinica* and *R. philippinarum*. A comprehensive analysis identified 540 acetylated proteins and 1639 acetylation sites, which were subsequently subjected to GO and KEGG enrichment analyses. The differentially expressed acetylated proteins were found to be primarily associated with biological processes such as glycolysis/gluconeogenesis, carbon fixation, ribosome, cGMP-PKG signaling pathway, among others.

Acetylation conservative motif analysis

The statistical analysis of amino acid preference or frequency of acetylation-modified peptide conserved motifs may reflect true preference [39]. In tea leaves, we observed that lysine (K), arginine (R), histidine (H), glutamic acid (E), aspartic acid (D), serine (S), and threonine (T) frequently occur at the +1 position in the motif. It is hypothesized that amino acid residues with alkaline or hydrophobic side chains may play a crucial role in acetylation [40]. Additionally, the three common motifs (K, H, and F) are present in the Gram-negative marine bacterium *Vibrio parahaemolyticus* [41]. Amino acids with large side chains, particularly tyrosine (Y) and phenylalanine (F), are predominantly enriched at the −2 and +1 positions in human cells [42]. In *A. longirostris*, motifs exhibit a preference for arginine (KacR), histidine (KacH), and lysine (KacK), most frequently at the +1 position. Acetylation in this species preferentially occurs in alkaline and positively charged amino acids [25]. The acetylation peptides of *A. marissinica* were subjected to motif enrichment analysis, revealing that the motifs -Arginine (KacR)-, -Threonine (KacT)-, and -Phenylalanine (KacF)- exhibited the highest frequency of occurrence. In these motifs, Arginine (R), Threonine (T), and Phenylalanine (F) are located at the +1 position, where Arg (R) is an alkaline amino acid, Thr (T) is a hydroxy amino acid, and Phe (F) is an aromatic amino acid. These findings suggest that acetylation preferentially occurs in regions containing alkaline, hydroxy, and aromatic amino acids in cold seep shellfish, which may play a significant role in the acetylation processes of *A. marissinica*.

Aceylated protein in glycolysis/gluconeogenesis and arginine kinase

Multiple enzymes involved in the KEGG pathway Glycolysis/Gluconeogenesis were displayed in Table S2 and Fig. 8, including pyruvate kinase, aldolase (ALDO), glyceraldehyde 3-phosphate dehydrogenase (GAPDH), and others. Notably, GAPDH is a crucial component of the glycolysis pathway [43]. A study comparing Rpgill and Amgill observed that GAPDH was acetylated and upregulated in Amgill (Fig. 8). This upregulation may facilitate the coupling of oxidative phosphorylation to ATP production by increasing NADH levels [43], allowing for adaptation to the low-temperature conditions of the cold seep zone. GAPDH acetylation had also been documented in other organisms such as *Escherichia coli* [44] and *Saccharopolyspora erythraea* [45], suggesting potential similar regulatory mechanisms. Furthermore, our study also revealed that the enzyme phosphoenolpyruvate carboxykinase, a key player in the gluconeogenesis pathway, was upregulated by acetylation in Amgill

(Fig. 8). This upregulation may increase glucose synthesis to fulfill metabolic demands via acetylation modification. It was also observed that the acetylation levels of KEGG pathway glycolysis/gluconeogenesis members were downregulated in Amgill (Ammuscle vs. Amgill), as shown in Table S3. This downregulation might be attributed to the presence of symbiotic bacteria in Amgill, which potentially supply energy and organic matter to the host [27], thereby inhibiting the acetylation level of glycolysis/gluconeogenesis members in Amgill.

The crucial enzyme involved in energy metabolism, arginine kinase, underwent acetylation modification. The acetylation levels of specific lysine residues in arginine kinases AmAK1 and AmAK2 (K316, K454, and K534 in AmAK1, K324 in AmAK2) were significantly upregulated in Amgill compared to Rpgill, as indicated in Table S6-1. Prior research has demonstrated the involvement of arginine kinase in reversible phosphorylation reactions, resulting in ATP production [46]. Additionally, a study revealed that acetylation of arginine kinase in *Solenopsis invicta* is linked to cellular energy metabolism and immune response [47]. It is suggested that the arginine kinase of Vesicomyid clam might enhance ATP production through acetylation to better adapt to the cold seep environment. In the comparison analysis between Ammuscle and Amgill, it was observed that only two sites (K454 and K534) in AmAK1 showed significant upregulation in Amgill (Table S6-2). Previous research has indicated that arginine kinase levels were notably higher in resistant silkworm larvae than susceptible larvae, suggesting a role for arginine kinase in the immune response [48, 49]. Our cold seep clam AK may also be involved in modulating its acetylation levels to interact with symbiotic bacteria.

A. marissinica' hemoglobin and acetylation modification

The uptake and conveyance of oxygen and sulfides are crucial processes for Vesicomyidae clams, with hemoglobin serving a significant function in these processes. Sequence alignment analysis revealed that the hemoglobin of Vesicomyid clams possesses heme contact residues (44 F and 90 H, as referenced in AmHbI) and ligand binding residues (30Y, 58Q, and 62 F, as referenced in AmHbI) (Fig. S7a), suggesting its capacity to engage in the binding and transport of oxygen in deep-sea mollusks. The comparison between the Rpgill and Amgill groups revealed that 15 acetylation sites of AmHbI exhibited significant upregulation in cold seep clam gill tissue, while one site displayed low expression (Table S6-1). This pattern was also observed in AmHbII. Prior research has indicated that acetylated hemoglobin was associated with enhanced oxygen affinity and decreased heme-heme interaction [50, 51]. The adaptation of cold seep clam hemoglobin to high hydrostatic pressure and low temperature might involve an increase in acetylation levels. Subsequent analyses revealed that all significantly differentially acetylated sites were situated within the alpha-helix region (Fig. S7c, d). Researchers also observed acetylation of hemocyanins, a respiratory protein found in deep sea shrimp *Alvinocaris longirostris*, with a greater number of acetylated sites located within secondary structures to enhance the stability of the hemocyanin complex [25]. Furthermore, the acetylation levels of AmHbI and AmHbII in the gill tissues of cold seep clams from the comparative group Ammuscle vs. Amgill were found to be significantly elevated, as indicated in Table S6-2. Given that deep-sea clam gill tissues harbor symbiotic bacteria dependent on sulfides for their survival, hemoglobin was implicated in sulfide transport through acetylation modifications to enhance transport efficiency [52, 53].

Stress adaptation acetylation protein-heat shock protein

Heat shock proteins are crucial in cellular responses to various stressors, including heat stimulus and osmotic pressure [54–56]. In the results section, it was observed that four heat shock proteins, namely Amhsp22, Amhsp70-1, Amhsp70-2, and Amhsp90, were acetylated. The acetylation levels of K100 and K111 in Amhsp22 and K246 in Amhsp70-2 were significantly elevated in the Amgill tissue (Rpgill vs. Amgill). A prior investigation demonstrated that following a 3-hour exposure to an extremely low-frequency electromagnetic field, cells displayed reduced expression of HSP70 and HSP90 proteins, yet their acetylation levels were increased, thereby promoting protein folding through the activation of HSP acetylation [57]. The hsp22 and hsp70 proteins found in cold seep clams might exhibit comparable mechanisms in response to extreme high-pressure and low-temperature conditions in deep-sea environments. This phenomenon was also observed in hsp70 proteins from deep-sea hydrothermal shrimp *Alvinocaris longirostris*, which have been identified as acetylated and implicated in adaptation to extreme high-pressure and high-temperature environments [25]. Within the Ammuscle versus Amgill comparison group, the acetylation levels of most sites from hsp22, hsp70-1, and hsp70-2 were downregulated in Amgill. Conversely, only K196 and K441 in hsp90 exhibited high expression levels in Amgill, both of which were situated within the alpha-helix region (Table S6-2 and Fig. S8e). Following the acetylation of hsp90 with lysine 60 derived from *Bombyx mori* silkworms, the activation of the JAK/STAT pathway occurred, resulting in a reduction of BmHSP90 ATPase activity and subsequent decrease in chaperone activity, ultimately inhibiting the proliferation of nucleopolyhedrovirus in *Bombyx mori*

(BmNPV) [58]. Given the presence of symbiotic bacteria in Amgill, Amhsp90 may play a crucial role in regulating symbiotic bacteria populations and maintaining homeostasis through acetylation of heat shock protein.

Acetylation modification of carbonic anhydrase and Ci fixation

Carbonic anhydrase (CA) is essential in inorganic carbon fixation and facilitates the transfer of inorganic carbon to symbionts within cold seep clams [59, 60]. Most inorganic carbon (i.e. CO_2 and HCO^-_3) predominantly exists in the form of bicarbonate (HCO^-_3) due to the pH of seawater, which hinders its passage through the cell membrane [61, 62]. Researchers discovered that host CAs in *Calyptogena* clams can catalyze the conversion of carbon dioxide and bicarbonate (converting HCO^-_3 into CO_2) within the clam hemolymph, thereby supplying intracellular CO_2 to symbiotic bacteria [59, 60]. The comparative proteomics analysis in cold seep clams revealed that CA exhibited elevated expression levels in Amgill (Ammantle/Amgill) [28]. Subsequent examination indicated that the acetylation levels of seven sites in Amca1 and approximately six sites in Amca2 were notably upregulated in Amgill (Table S6-1, Rpgill/Amgill) in the present investigation. A similar situation was observed in the comparative group of Ammuscle vs. Amgill, where approximately eight sites in Amca1 and about seven sites in Amca2 were significantly upregulated in Amgill (Table S6-2, Ammuscle/Amgill). Previous studies had demonstrated that acetylation of bovine CA II was essential for modulating protein-protein interactions through the promotion of polar residues, particularly acetylated lysine, at molecular interfaces while diminishing the influence of non-polar residues in these contact regions [63–65]. Based on the analysis above, it is hypothesized that CA may potentially augment its catalytic activity in the interaction with CO_2 or HCO^-_3 by means of a substantial presence of acetylated lysine on the interface. In facilitating the provision of inorganic carbon to symbiotic bacteria, the host's CA might not only upregulate protein expression [28], but also via protein acetylation. Further validation is needed in subsequent studies.

Myosin-the protein with the highest number of acetylation sites

Myosin, the primary constituent of thick filaments in skeletal muscle, facilitates the cyclic interaction process between myosin and actin through the presence of myosin heavy chains [66, 67]. Our research findings demonstrate that myosin heavy chain (Ama01085) possessed the highest number of acetylation sites (149 sites), with 14 sites showing significant upregulation in Amgill (Rpgill/Amgill, Table S6-1). Prior studies have demonstrated that the acetylation of myosin heavy chain and actin is crucial in regulating the interaction between myosin and actin by inhibiting their phosphorylation, consequently impeding the dissociation of actomyosin. This acetylation process has been displayed to decrease the overall energy of the actomyosin system and enhance its stability [68, 69]. Given the variance in hydrostatic pressure between cold seep clam and *Ruditapes philippinarum*, it is plausible that similar mechanisms may be employed to reduce system energy and promote actomyosin' stability in *A. marissinica*. We also observed a decrease in the acetylation levels of 55 sites in the Amgill (Ammuscle/Amgill, Table S6-2). Given the abundance of myosin and actin in the adductor muscle, additional analysis (hydrostatic pressure experiment, etc.) was warranted to elucidate the potential implications of myosin' acetylation modifications in Ammuscle.

Conclusion

This research presented the initial comparative analysis of lysine acetylation patterns between *A. marissinica* and *R. philippinarum*. A total of 1634 acetylation sites on 539 modified proteins were quantified, identifying three predominant consensus motifs: -KacR-, -KacT-, and -KacF-. The proteins containing differentially expressed modified peptides underwent GO and KEGG analyses. The GO enrichment analysis revealed that acetylated proteins were involved in various biological processes, including cellular response to stimulation, guanyl riboside binding, GTP binding, nucleoside binding, cytoskeleton organization, and other cellular processes. KEGG enrichment analysis showed that the acetylation protein was involved in diverse pathways, such as tight junction, motor proteins, gap junction, phagosome, cGMP PKG signaling pathway, endocytosis, glycolysis/gluconeogenesis, among others. Significantly, abundant lysine acetylation was identified within the glycolysis/gluconeogenesis pathway. Additionally, acetylation linked to adaptation to deep-sea environments was also observed, with specific characterization of key proteins including arginine kinase, hemoglobin, heat shock protein, carbonic anhydrase, and myosin heavy chain. Thus, our research offers valuable insights into the role of reversible lysine acetylation in marine invertebrates, particularly in understanding the adaptation mechanisms of *A. marisinica* and other deep-sea mollusks to cold seep environments.

Abbreviations

AK	Arginine kinase
CA	Carbonic anhydrase
GO	Gene Ontology
GAPDH	Glyceraldehyde 3-phosphate dehydrogenase
Hb	Hemoglobin
hsp	heat shock proteins
Ci	Inorganic carbon
KEGG	Kyoto Encyclopedia of Genes and Genomes
LC-MS/MS	Liquid chromatography-mass spectrometry/mass spectrometry
PCR	Polymerase chain reaction

Supplementary Information

The online version contains supplementary material available at https://doi.org/10.1186/s12864-024-10916-9.

Supplementary Material 1: Fig. S1. The Venn diagram of the peptides and proteins containing acetylation sites in *Archivesica marissinica* and *Ruditapes philippinarum* (Intragroup comparison). **a1, b1, c1** The Venn diagram of the peptides containing acetylation sites. **a2, b2, c2** The Venn diagram of the proteins containing acetylation sites.

Supplementary Material 2: Fig. S2. Subcellular localization and domain analysis of the differentially expressed acetylated proteins for *Archivesica marissinica*' muscle (Ammuscle) vs.Archivesica marissinica'gill (Amgill).a Subcellular localization of the differential expressedacetylated proteins.b Domain enrichment analysis of the differential expressedacetylated proteins.

Supplementary Material 3: Fig. S3. GO analysis related maps o of the differentially expressedacetylated proteins for *Archivesica marissinica*'muscle (Ammuscle) vs. *Archivesica marissinica*'gill (Amgill). **a1, a2,a3** Biological process enrichment bubble map of all differential proteins, upregulated proteins and downregulated proteins, respectively. **b1, b2, b3** Molecular function enrichment bubble map of all differential proteins, upregulated proteins and downregulated proteins, respectively. **c1, c2, c3** Cellular component enrichment bubble map of all differential proteins, upregulated proteins and downregulated proteins, respectively.

Supplementary Material 4: Fig. S4. Kyoto Encyclopedia of Genes and Genomes pathway analysis of the differentially expressedacetylated proteins for *Archivesica marissinica*'muscle (Ammuscle) vs. *Archivesica marissinica*'gill (Amgill). **a1, a2, a3** KEGG pathway enrichment bubble map of all differential proteins, upregulated proteins and downregulated proteins, respectively.

Supplementary Material 5: Fig. S5. Protein interaction network of differentially expressed acetylated proteins from Ammuscle vs. Amgill. **a** Protein interaction network of all differentially expressed acetylated proteins, **b, c, d, e, f** Protein interaction network of five distinct clusters.

Supplementary Material 6: Fig. S6. Sequence alignment, evolutionary tree, and tertiary structure of carbonic anhydrase (ca) from selected mollusks species. **a** Sequence alignment of arginine kinases from *Archivesica marissinica* (Amca1, Ama18071; Amca2, Ama18072), *Phreagena okutanii* (Poca, BAO01208.1),*Archivesica packardana* (Apca, QFP92276.1), *Mercenaria mercenaria* (Mmca,XP_045193509.1), *Ruditapes philippinarum* (Rpca, XP_060586828.1), *Mya arenaria* (Maca, XP_052815146.1)**b** Phylogenetic tree of carbonic anhydrase from *Archivesica marissinica* (Amca1, Ama18071; Amca2, Ama18072), *Phreagena okutanii* (Po2dca, BAU71500.1; Poca, BAO01208.1), *Archivesica packardana* (Ap2dca, QFP92274.1; Apca, QFP92276.1), *Mercenaria mercenaria* (Mm2dca, XP_045171808.2; Mmca,XP_045193509.1), *Ruditapes philippinarum* (Rp2dca, XP_060574644.1; Rpca, XP_060586828.1), *Dreissena polymorpha* (Dp2dcax1, XP_052270369.1; Dp2dca,XP_052270366.1), *Tridacna squamosa* (Ts2dca, ATC20500.1), *Tridacna gigas* (Tg2dca, AAX16122.1), *Mya arenaria* (Maca, XP_052815146.1). **c d** Predicted tertiary structure of Amca1 and Amca2, respectively. The acetylation sites and N, C terminal of proteins are marked in red.

Supplementary Material 7: Fig. S7. Sequence alignment, evolutionary tree, and tertiary structure of hemoglobin (Hb) from selected mollusks species. **a** Sequence alignment of arginine kinases from *Archivesica marissinica* (AmHbI, Ama28498; AmHbII, Ama33183), *Phreagena soyoae* (PsHb-I, BAD34603.1; PsHb-II, BAD34604.1), *Calyptogena kaikoi* (CkaHb-I, BAD34601.1; CkaHb-I, BAD34602.1), *Calyptogena nautilei* (CnaHb-III, BAD34605.1; CnaHb-IV, BAD34606.1), *Calyptogena tsubasa* (CtsHb-I, BAD35020.1; CtsHb-II, BAD35021.1), *Archivesica packardana* (ApHb-I, ApHb-II, ApHb-IIIa, ApHb-IIIb, SRR8820491, SRR8820490, re-assemble), *Calyptogena magnifica* (CmagHb-I, CmagHb-II, CmagHb-IIIa, CmagHb-IIIb, SRR8217831, re-assemble), *Phreagena okutanii* (PoHb-I, PoHb-II, PoHb-IIIa, PoHb-IIIb, SRR7156763, SRR7156764, re-assemble). Heme contact residues and ligand binding residues are marked in red.**b** Phylogenetic tree of hemoglobin. **cd** Predicted tertiary structure of AmHb-I and AmHb-II, respectively. The acetylation sites and N, C terminal of proteins are marked in red.

Supplementary Material 8: Fig. S8. Evolutionary tree and tertiary structure of heat shock protein (hsp) from selected mollusks species. **a** Evolutionary tree of arginine kinases from *Archivesica marissinica* (Amhsp22, Ama24071; Amhsp70-1, Ama03033; Amhsp70-2, Ama15332; Amhsp90, Ama08855), *Mercenaria mercenaria* (Mmhsp27, XP_045176285.1; Mmhsp70, XP_045202781.2; Mmhsp90, XP_045185402.2), *Ruditapes philippinarum* (Rphspbeta6, XP_060568939.1; Rphsp22, ACU83231.1; Rphsp70-12a, XP_060570239.1; Rphsp70, AHY27547.1; Rphsp90, XP_060560332.1), *Meretrix meretrix* (Mmehsp20, AFK80359.1; Mmehsp70, ADT78476.1), *Cyclina sinensis* (Cshsp20, AET13647.1; Cshsp70, AET13646.3), *Mya arenaria* (Mahspbeta6, XP_052798161.1; Mahsp70, XP_052794101.1; Mahsp70x2, XP_052805112.1), *Dreissena polymorpha* (Dphsp70, XP_052280349.1; Dphsp90, XP_052275659.1), *Ostrea edulis* (Oehsp70, XP_048773133.1), *Corbicula fluminea* (Cfhsp70, AHY03302.1; Cfhsp90, AMM04544.1), *Sinonovacula constricta* (Schsp90, QDG10047.1).**b c d e** Predicted tertiary structure of Amhsp22, Amhsp70-1, Amhsp70-2, and Amhsp90, respectively. The acetylation sites and N, C terminal of proteins are marked in red.

Supplementary Material 9: Fig. S9. Evolutionary tree and tertiary structure of myosin heavy chain (MyHC) from selected mollusks species. **a** Evolutionary tree of myosin heavy chain from *Archivesica marissinica* (AmMyHC1, Ama01085; AmMyHC2, Ama02678; AmMyHC3, Ama01076; AmMyHC4, Ama00622), *Mercenaria mercenaria* (MmMyHC, XP_045214006.2; MmMyHCnm, XP_053393241.1), *Ruditapes philippinarum* (RpMyHC, XP_060584784.1; RpMyHCnm, XP_060570204.1), *Mya arenaria* (MaMyHC, XP_052814202.1; MaMyHCnm, XP_052769024.1), *Dreissena polymorpha* (DpMyHC, XP_052236757.1; DpMyHCnm, XP_052263231.1), *Pecten maximus* (PmMyHC, XP_033742374.1; PmMyHCnm, XP_033747857.1).**b cd e** Predicted tertiary structure of AmMyHC1-4, respectively. The acetylation sites and N, C terminal of proteins are marked in red.

Supplementary Material 10: Table S1. Acetylated proteins and sites from comparative groups Rpgill vs. Amgill, Ammuscle vs. Amgill.

Supplementary Material 11: Table S2. Acetylated proteins involved in differentially significantly KEGG pathway from comparative group Rpgill vs. Amgill.

Supplementary Material 12: Table S3. Acetylated proteins involved in differentially significantly KEGG pathway from comparative group Ammuscle vs. Amgill.

Supplementary Material 13. Table S4. Acetylated proteins involved in protein interaction of the comparative group Rpgill vs. Amgill.

Supplementary Material 14. Table S5. Acetylated proteins involved in protein interaction of the comparative group Ammuscle vs. Amgill.

Supplementary Material 15: Table S6. Specific acetylation proteins and acetylation sites from comparative group Rpgill vs. Amgill, Ammuscle vs. Amgill.

Supplementary Material 16: Table S7. Sequence information for sequence alignment and evolutionary tree.

Supplementary Material 17: Table S8. All identified proteins and their expression levels.

Acknowledgements
Samples were collected on board of "Explorer 1" scientific research ship of Institute of Deep-sea Science and Engineering (Chinese Academy of Sciences) by using "Deep-sea Warrior" manned submersible, we thank the crew for their help during the cruise.

Authors' contributions
XK performed most of the experiments, analyzed data, and wrote the manuscript. XS planned and designed the research. XS and HZ revised the manuscript. WW, SC, MS, YZ, YC and XS assisted in the experiment. All authors contributed to the article and approved the submitted version.

Funding
This work was supported by Natural Science Foundation of Jiangsu Province (Grant No. BK20210927), National Nature Science Foundation of China (Grant

No. 42376139), Jiangsu Agriculture Science and Technology Innovation Fund (JASTIF) (CX(22)2032), Strategic Priority Research Program of the Chinese Academy of Sciences (CAS) (XDA22050303).

Data availability
Data is provided within the manuscript or supplementary information files.

Declarations

Ethics approval and consent to participate
Not applicable.

Consent for publication
Not applicable.

Competing interests
The authors declare no competing interests.

Author details
[1]School of Marine Science and Fisheries, Jiangsu Ocean University, Lianyungang 222000, China. [2]Co-Innovation Center of Jiangsu Marine Bio-Industry Technology, Jiangsu Ocean University, Lianyungang 222000, China. [3]Institute of Deep-sea Science and Engineering, Chinese Academy of Sciences, Sanya 572000, China.

Received: 31 May 2024 Accepted: 17 October 2024
Published online: 28 October 2024

References

1. Thurber AR, Sweetman AK, Narayanaswamy BE, Jones DOB, Ingels J, Hansman RL. Ecosystem function and services provided by the deep sea. Biogeosciences. 2014;11(14):3941–63.
2. La Cono V, Ruggeri G, Azzaro M, Crisafi F, Decembrini F, Denaro R, La Spada G, Maimone G, Monticelli LS, Smedile F, Giuliano L, Yakimov MM. Contribution of bicarbonate assimilation to carbon pool dynamics in the deep mediterranean sea and cultivation of actively nitrifying and CO(2)-fixing bathypelagic prokaryotic consortia. Front Microbiol. 2018;9:3–7.
3. Bettencourt R, Roch P, Stefanni S, Rosa D, Colaco A, Santos RS. Deep sea immunity: unveiling immune constituents from the hydrothermal vent mussel Bathymodiolus Azoricus. Mar Environ Res. 2007;64(2):108–27.
4. Nussbaumer AD, Fisher CR, Bright M. Horizontal endosymbiont transmission in hydrothermal vent tubeworms. Nature. 2006;441(7091):345–8.
5. Nègre-Sadargues G, Castillo R, Segonzac M. Carotenoid pigments and trophic behaviour of deep-sea shrimps (Crustacea, Decapoda, Alvinocarididae) from a hydrothermal area of the mid-atlantic ridge. Comp Biochem Physiol Mol Integr Physiol. 2000;127(3):293–300.
6. Cartes JE, Maynou F, Abelló P, Emelianov M, de Sola LG, Solé M. Long-term changes in the abundance and deepening of the deep-sea shrimp Aristaeomorpha foliacea in the Balearic Basin: relationships with hydrographic changes at the Levantine Intermediate Water. J Mar Syst. 2011;88(4):516–25.
7. Vrijenhoek RC. Genetics and Evolution of Deep-Sea Chemosynthetic Bacteria and TheirInvertebrate Hosts. In: Kiel S, editor. The Vent and Seep Biota: Aspects from Microbes to Ecosystems. Dordrecht: Springer, Netherlands; 2010. p. 15–49.
8. Paull CK, Hecker B, Commeau R, Freeman-Lynde RP, Neumann C, Corso WP, Golubic S, Hook JE, Sikes E, Curray J. Biological communities at the Florida escarpment resemble hydrothermal vent taxa. Science. 1984;226(4677):965–7.
9. German CR, Ramirez-Llodra E, Baker MC, Tyler PA. Deep-water chemosynthetic ecosystem research during the census of marine life decade and beyond: a proposed deep-ocean road map. PLoS ONE. 2011;6(8): e23259.
10. Danovaro R, Snelgrove PV, Tyler P. Challenging the paradigms of deep-sea ecology. Trends Ecol Evol. 2014;29(8):465–75.
11. Downing AB, Wallace GT, Yancey PH. Organic osmolytes of amphipods from littoral to hadal zones: increases with depth in trimethylamine N-oxide, scyllo-inositol and other potential pressure counteractants. Deep Sea Res Part I Oceanogr Res Pap. 2018;138:23–30.
12. Sanders NK, Childress JJ. Adaptations to the deep-sea oxygen minimum layer: oxygen binding by the hemocyanin of the bathypelagic mysid, gnathophausia ingens dohrn. Biol Bull. 1990;178(3):286–94.
13. Dubilier N, Bergin C, Lott C. Symbiotic diversity in marine animals: the art of harnessing chemosynthesis. Nat Rev Microbiol. 2008;6(10):725–40.
14. Sun Y, Wang M, Zhong Z, Chen H, Wang H, Zhou L, Cao L, Fu L, Zhang H, Lian C, Sun S, Li C. Adaption to hydrogen sulfide-rich environments: strategies for active detoxification in deep-sea symbiotic mussels, Gigantidas platifrons. Sci Total Environ. 2022;804: 150054.
15. Mann M, Jensen ON. Proteomic analysis of post-translational modifications. Nat Biotechnol. 2003;21(3):255–61.
16. Gershey EL, Vidali G, Allfrey VG. Chemical studies of histone acetylation. The occurrence of epsilon-N-acetyllysine in the f2a1 histone. J Biol Chem. 1968;243(19):5018–22.
17. Koprinarova M, Schnekenburger M, Diederich M. Role of histone acetylation in cell cycle regulation. Curr Top Med Chem. 2016;16(7):732–44.
18. Li P, Ge J, Li H. Lysine acetyltransferases and lysine deacetylases as targets for cardiovascular disease. Nat Rev Cardiol. 2020;17(2):96–115.
19. Shen Z, Wang B, Luo J, Jiang K, Zhang H, Mustonen H, Puolakkainen P, Zhu J, Ye Y, Wang S. Global-scale profiling of differential expressed lysine acetylated proteins in colorectal cancer tumors and paired liver metastases. J Proteom. 2016;142:24–32.
20. Shen M, Chen Z, Ming M, Cheng Z, Sun J, Liang Q, Shang T, Zhang Q, Zhou S, Ji Y, Ding F. The acetylome of adult mouse sciatic nerve. J Neurochem. 2022;162(3):262–75.
21. Meng X, Lv Y, Mujahid H, Edelmann MJ, Zhao H, Peng X, Peng Z. Proteome-wide lysine acetylation identification in developing rice (Oryza sativa) seeds and protein co-modification by acetylation, succinylation, ubiquitination, and phosphorylation. Biochim Biophys Acta. 2018;1866(3):451–63.
22. Li BB, Zhang W, Wei S, Lv YY, Shang JX, Hu YS. Comprehensive proteome and lysine acetylome analysis after artificial aging reveals the key acetylated proteins involved in wheat seed oxidative stress response and energy production. J Food Biochem. 2022;46(12):e14495.
23. Lv Y. Proteome-wide profiling of protein lysine acetylation in aspergillus flavus. PLoS ONE. 2017;12(6): e0178603.
24. Wang T, Guan W, Du Y, Xu Y, He Z, Zhang Y, Kang C, Wan X, Chi X, Sun K, Zhang X. Proteome-wide analyses reveal diverse functions of acetylation proteins in Neurospora Crassa. Proteomics. 2021;21(6):e2000212.
25. Hui M, Cheng J, Sha Z. First comprehensive analysis of lysine acetylation in Alvinocaris Longirostris from the deep-sea hydrothermal vents. BMC Genomics. 2018;19(1):352–65.
26. Lan Y, Sun J, Zhang W, Xu T, Zhang Y, Chen C, Feng D, Wang H, Tao J, Qiu J-W, Qian P-Y. Host–symbiont interactions in deep-sea chemosymbiotic vesicomyid clams: insights from transcriptome sequencing. Front Mar Sci. 2019;6:3–9.
27. Ip JC, Xu T, Sun J, Li R, Chen C, Lan Y, Han Z, Zhang H, Wei J, Wang H, Tao J, Cai Z, Qian PY, Qiu JW. Host-endosymbiont genome integration in a deep-sea chemosymbiotic clam. Mol Biol Evol. 2021;38(2):502–18.
28. Kong X, Wang W, Chen S, Mao N, Cai Y, Li Y, Xia S, Zhang H, Shen X. Comparative proteomic analysis of cold seep clam Archivesica Marissinica and shallow water shellfish Ruditapes philippinarum provides insights into the adaptation mechanisms of deep-sea mollusks. Front Mar Sci. 2024;10: 1294736.
29. Johnson SB, Krylova EM, Audzijonyte A, Sahling H, Vrijenhoek RC. Phylogeny and origins of chemosynthetic vesicomyid clams. Syst Biodivers. 2016;15(4):346–60.
30. Tan Y, Fang L, Qiu M, Huo Z, Yan X. Population genetics of the Manila clam (Ruditapes Philippinarum) in East Asia. Sci Rep. 2020;10(1):21890.
31. Folmer O, Black M, Hoeh W, Lutz R, Vrijenhoek R. DNA primers for amplification of mitochondrial cytochrome c oxidase subunit I from diverse metazoan invertebrates. Mol Mar Biol Biotechnol. 1994;3(5):294–9.
32. Wiśniewski JR, Zougman A, Nagaraj N, Mann M. Universal sample preparation method for proteome analysis. Nat Methods. 2009;6(5):359–62.
33. Zhang J, Xin L, Shan B, Chen W, Xie M, Yuen D, Zhang W, Zhang Z, Lajoie GA, Ma B. PEAKS DB: de novo sequencing assisted database search for sensitive and accurate peptide identification. Mol Cell Proteom. 2012;11(4):67–75.
34. Yu CS, Cheng CW, Su WC, Chang KC, Huang SW, Hwang JK, Lu CH. CELLO2GO: a web server for protein subCELlular LOcalization prediction with functional gene ontology annotation. PLoS ONE. 2014;9(6): e99368.

35. Mistry J, Chuguransky S, Williams L, Qureshi M, Salazar GA, Sonnhammer ELL, Tosatto SCE, Paladin L, Raj S, Richardson LJ, Finn RD, Bateman A. Pfam: the protein families database in 2021. Nucleic Acids Res. 2021;49(D1):D412-9.
36. Shannon P, Markiel A, Ozier O, Baliga NS, Wang JT, Ramage D, Amin N, Schwikowski B, Ideker T. Cytoscape: a software environment for integrated models of biomolecular interaction networks. Genome Res. 2003;13(11):2498–504.
37. Larkin MA, Blackshields G, Brown NP, Chenna R, McGettigan PA, McWilliam H, Valentin F, Wallace IM, Wilm A, Lopez R, Thompson JD, Gibson TJ, Higgins DG. Clustal W and Clustal X version 2.0. Bioinformatics. 2007;23(21):2947–8.
38. Kumar S, Stecher G, Li M, Knyaz C, Tamura K. MEGA X: molecular evolutionary genetics analysis across computing platforms. Mol Biol Evol. 2018;35(6):1547–9.
39. Li P, Chen C, Li P, Dong Y. A comprehensive examination of the lysine acetylation targets in paper mulberry based on proteomics analyses. PLoS ONE. 2021;16(3): e0240947.
40. Jiang J, Gai Z, Wang Y, Fan K, Sun L, Wang H, Ding Z. Comprehensive proteome analyses of lysine acetylation in tea leaves by sensing nitrogen nutrition. BMC Genomics. 2018;19(1):840.
41. Pan J, Chen R, Li C, Li W, Ye Z. Global analysis of protein lysine succinylation profiles and their overlap with lysine acetylation in the marine bacterium vibrio parahemolyticus. J Proteome Res. 2015;14(10):4309–18.
42. Choudhary C, Kumar C, Gnad F, Nielsen ML, Rehman M, Walther TC, Olsen JV, Mann M. Lysine acetylation targets protein complexes and co-regulates major cellular functions. Science. 2009;325(5942):834–40.
43. Nelson DL, Lehninger AL, Cox MM. Lehninger principles of biochemistry. London: Macmillan; 2008.
44. Zhang J, Sprung R, Pei J, Tan X, Kim S, Zhu H, Liu CF, Grishin NV, Zhao Y. Lysine acetylation is a highly abundant and evolutionarily conserved modification in Escherichia coli. Mol Cell Proteom. 2009;8(2):215–25.
45. Kim SC, Sprung R, Chen Y, Xu Y, Ball H, Pei J, Cheng T, Kho Y, Xiao H, Xiao L, Grishin NV, White M, Yang XJ, Zhao Y. Substrate and functional diversity of lysine acetylation revealed by a proteomics survey. Mol Cell. 2006;23(4):607–18.
46. Uda K, Yamamoto K, Iwasaki N, Iwai M, Fujikura K, Ellington WR, Suzuki T. Two-domain arginine kinase from the deep-sea clam Calyptogena kaikoi-evidence of two active domains. Comp Biochem Physiol B Biochem Mol Biol. 2008;151(2):176–82.
47. Ye J, Li J. First proteomic analysis of the role of lysine acetylation in extensive functions in Solenopsis invicta. PLoS ONE. 2020;15(12): e0243787.
48. Kang L, Shi H, Liu X, Zhang C, Yao Q, Wang Y, Chang C, Shi J, Cao J, Kong J, Chen K. Arginine kinase is highly expressed in a resistant strain of silkworm (Bombyx mori, Lepidoptera): implication of its role in resistance to Bombyx mori nucleopolyhedrovirus. Comp Biochem Physiol B Biochem Mol Biol. 2011;158(3):230–4.
49. Yanan Z, Peixuan L, Yong S, Lichun F. Advances in the research of arginine kinase in insects. Acta Entomol Sin. 2018;61(3):385–90.
50. Bridges KR, Schmidt GJ, Jensen M, Cerami A, Bunn HF. The acetylation of hemoglobin by aspirin. In vitro and in vivo. J Clin Invest. 1975;56(1):201–7.
51. Xu ASL, Ohba Y, Vida L, Labotka RJ, London RE. Aspirin acetylation of βLys-82 of human hemoglobin: NMR study of acetylated hemoglobin tsurumai. Biochem Pharmacol. 2000;60(7):917–22.
52. Suzuki T, Kawamichi H, Ohtsuki R, Iwai M, Fujikura K. Isolation and cDNA-derived amino acid sequences of hemoglobin and myoglobin from the deep-sea clam Calyptogena kaikoi. Biochim Biophys Acta. 2000;1478(1):152–8.
53. Decker C, Zorn N, Le Bruchec J, Caprais JC, Potier N, Leize-Wagner E, Lallier FH, Olu K, Andersen AC. Can the hemoglobin characteristics of vesicomyid clam species influence their distribution in deep-sea sulfide-rich sediments? A case study in the Angola Basin. Deep Sea Res II:Top Stud Oceanogr. 2017;142:219–32.
54. Kurzik-Dumke U, Lohmann E. Sequence of the new Drosophila melanogaster small heat-shock-related gene, lethal(2) essential for life [l(2)efl], at locus 59F4,5. Gene. 1995;154(2):171–5.
55. Hui M, Liu Y, Song C, Li Y, Shi G, Cui Z. Transcriptome changes in Eriocheir sinensis megalopae after desalination provide insights into osmoregulation and stress adaption in larvae. PLoS ONE. 2014;9(12):e114187.
56. Zhang Y, Sun J, Mu H, Li J, Zhang Y, Xu F, Xiang Z, Qian PY, Qiu JW, Yu Z. Proteomic basis of stress responses in the gills of the pacific oyster Crassostrea gigas. J Proteome Res. 2015;14(1):304–17.
57. Huang Z, Ito M, Zhang S, Toda T, Takeda JI, Ogi T, Ohno K. Extremely low-frequency electromagnetic field induces acetylation of heat shock proteins and enhances protein folding. Ecotoxicol Environ Saf. 2023;264: 115482.
58. Zhang X, Ma S, Gu C, Hu M, Miao M, Quan Y, Yu W. K64 acetylation of heat shock protein 90 suppresses nucleopolyhedrovirus replication in Bombyx mori. Arch Insect Biochem Physiol. 2024;115(1): e22079.
59. Hongo Y, Nakamura Y, Shimamura S, Takaki Y, Uematsu K, Toyofuku T, Hirayama H, Takai K, Nakazawa M, Maruyama T, Yoshida T. Exclusive localization of carbonic anhydrase in bacteriocytes of the deep-sea clam Calyptogena okutanii with thioautotrophic symbiotic bacteria. J Exp Biol. 2013;216(Pt 23):4403–14.
60. Hongo Y, Ikuta T, Takaki Y, Shimamura S, Shigenobu S, Maruyama T, Yoshida T. Expression of genes involved in the uptake of inorganic carbon in the gill of a deep-sea vesicomyid clam harboring intracellular thioautotrophic bacteria. Gene. 2016;585(2):228–40.
61. Siegenthaler U, Sarmiento JL. Atmospheric carbon dioxide and the ocean. Nature. 1993;365(6442):119–25.
62. Geers C, Gros G. Carbon dioxide transport and carbonic anhydrase in blood and muscle. Physiol Rev. 2000;80(2):681–715.
63. Gudiksen KL, Gitlin I, Yang J, Urbach AR, Moustakas DT, Whitesides GM. Eliminating positively charged lysine epsilon-NH3 + groups on the surface of carbonic anhydrase has no significant influence on its folding from sodium dodecyl sulfate. J Am Chem Soc. 2005;127(13):4707–14.
64. Kang K, Choi JM, Fox JM, Snyder PW, Moustakas DT, Whitesides GM. Acetylation of Surface lysine groups of a protein alters the organization and composition of its crystal contacts. J Phys Chem B. 2016;120(27):6461–8.
65. Di Fiore A, Supuran CT, Scaloni A, De Simone G. Post-translational modifications in tumor-associated carbonic anhydrases. Amino Acids. 2022;54(4):543–58.
66. Szent-Györgyi AG. The early history of the biochemistry of muscle contraction. J Gen Physiol. 2004;123(6):631–41.
67. Lewis CTA, Ochala J. Myosin heavy chain as a novel key modulator of striated muscle resting state. Physiol (Bethesda). 2023;38(1):123–33.
68. Zhang Y, Li X, Zhang D, Bai Y, Wang X. Effects of acetylation on dissociation and phosphorylation of actomyosin in postmortem ovine muscle during incubation at 4°C in vitro. Food Chem. 2021;356: 129696.
69. Zhang Y, Li X, Zhang D, Ren C, Bai Y, Ijaz M, Wang X, Zhao Y. Acetylation of sarcoplasmic and myofibrillar proteins were associated with ovine meat quality attributes at early postmortem. Food Sci Anim Resour. 2021;41(4):650–63.

Publisher's note